Review

For reprint orders, please contact: reprints@futuremedicine.com

Nanomedicine

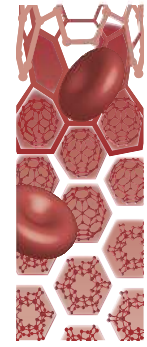

Recent progress in nanoscale metal-organic frameworks for drug release and cancer therapy

Liangcan He[1,2], Yuan Liu[2], Joseph Lau[2], Wenpei Fan[2], Qunying Li[1], Chao Zhang[1], Pintong Huang*[,1] & Xiaoyuan Chen**[,2]

[1]Department of Ultrasound in Medicine, The Second Affiliated Hospital of Zhejiang University School of Medicine, Zhejiang 310009, PR China

[2]Laboratory of Molecular Imaging & Nanomedicine, National Institute of Biomedical Imaging & Bioengineering, National Institutes of Health, Bethesda, MD 20892, USA

*Author for correspondence: huangpintong@zju.edu.cn

**Author for correspondence: shawn.chen@nih.gov

Nanoscale metal-organic frameworks (MOFs) have been widely used as controlled drug delivery vehicles and cancer therapy agents due to their intrinsic superior properties. Scientists have made remarkable achievements in the field of nanomedicine by using the MOFs and MOF-based multifunctional nanomaterials due to the easy synthesis into nanoscale and functionalization. In this review, we highlight the recent progress of nanoscale MOFs as drug delivery vehicles for cancer theranostics. We divide the discussion into three parts. The first and second parts focus on the drug delivery of unmodified MOF and modified MOFs, respectively, while the third part focuses on porphyrin MOFs as photosensitizers for photodynamic therapy. Finally, we conclude by identifying areas of research that we believe will propel the translation and application of MOFs.

First draft submitted: 16 September 2018; Accepted for publication: 20 March 2019; Published online: 14 May 2019

Keywords: *in situ* drug encapsulation • nanoscale metal-organic frameworks • photodynamic therapy • porphyrinic metal-organic frameworks • stimuli-responsive drug release

With the rapid development of nanoscience and technology, there has been an increasing focus on multifunctional therapeutic agents that can detect and treat cancer *in vivo*. Cancer causes millions of deaths annually and is the second leading cause of death in humans. Chemotherapy, a conventional treatment modality, has intrinsic limitations including serious side effects, drug resistance, uncontrollable release and poor tumor accumulation [1]. As a result, much effort has been devoted to the development of nanocarriers for controllable drug release and cancer therapy in order to minimize side effects and improve therapeutic efficacy. Recently, different kinds of drug carriers were used for this purpose, such as porous silica, DNA, micelles, liposomes, dendrimers, metal nanoparticles and quantum dots [2–15]. However, most of these nanocarriers have drawbacks, such as limited drug-loading efficiency, high toxicity and poor biocompatibility. Ideally, the nanocarriers should have low toxicity, high drug-loading capacity, good biocompatibility and easy biodegradability or excretion. Furthermore, the nanocarriers should have minimum premature drug release with a controlled release mechanism.

Metal-organic frameworks (MOFs), an emerging class of porous crystalline material assembled from metal containing node (e.g., metal ions or clusters) and organic ligands (e.g., carboxylate ligand or other negatively charged ligand), have gained popularity as a delivery vector. MOFs exhibit large surface areas, well-defined pore structures, tunable structures and pore sizes, functional versatility and good biocompatibility [16–21]. Many advances have been made in the field of MOF-based nanomedical applications, owing to facile size-controllable synthesis and functionalization via inclusion and surface chemistry. The MOF-based multifunctional platforms integrate the efficiency of multifunctional units to serve the specific purposes, fulfilling the increasing requirements and therapy tasks [22]. Compared with the traditional nanomaterials such as porous silica, MOFs have superior intrinsic properties [23,24]. First, MOFs have large surface areas that enable them to have high drug-loading capacity.

Future Medicine

Second, their versatile and tunable structures allow users to obtain particles with desired morphologies, sizes and/or compositions. Third, MOFs exhibit good biocompatibility and can be easily functionalized or modified through the attached ligands or metal containing node. Notably, the moderate coordination interaction between the organic ligands and the metal nodes makes the MOF materials biodegradable upon exposure to the tumor microenvironment. Furthermore, the versatile MOF chemistry provides ways to control and tune the host–guest interactions between the MOFs and the release probe molecules [25,26].

Individual nanoscale MOF for drug delivery

Drug loading with the postencapsulation method

Due to the intrinsic pore structures, the drugs with sizes smaller than the MOFs pore sizes could be easily entrapped by the MOFs by mixing the drugs and MOFs (named as the postencapsulation method). Due to the simplicity, this method has been widely used for loading various drugs/proteins into the porous MOF materials. In 2006, Férey and colleagues leveraged MOF materials as drug carriers and controlled delivery for the first time [27]. In their studies, ibuprofen (IBU) was encapsulated in cubic zeotypic metal carboxylates chromium-based MOFs, Materials of Institute Lavoisier (MIL)-100 (3340 m^2/g) and MIL-101 (5510 m^2/g), which were built from di- or tricarboxylic acids and trimers of metal octahedral. Both the MIL-100 and MIL-101 showed remarkable IBU adsorption: 0.35 g of IBU/g for MIL-100 and 1.4 g of IBU/g for MIL-101. From the kinetic release studies, the complete IBU release from MIL-100 and MIL-101 was achieved in 3 and 6 days, respectively. The authors also analyzed three different types of interactions during the IBU release process: relatively strong electrostatic interaction between the ligand and the IBU molecular, π–π interaction between the ligand and the IBU, and the weak IBU–IBU interactions. Despite the differences in cage size and strong interaction IBU, comparable dosage and kinetics were observed in the MIL-100 and MIL-101 compared with porous MCM-41 [28]. Importantly, this work demonstrated a noncovalent encapsulation method using MOF materials for drug delivery and controlled release.

Taking the toxicity of the chromium compounds into consideration, other research groups pursued other low metal ions or used cluster-constructed MOF nanomaterials [19,29]. In 2010, Horcajada *et al.* systematically explored the drug release in several iron (III) carboxylate MOFs (MIL-53, MIL-88A, MIL-88B, MIL-89, MIL-100 and MIL-101) [19]. Several efficient anticancer and antiviral drugs, such as doxorubicin (DOX), azidothymidine triphosphate and cidofovir, were encapsulated in the iron carboxylate MOFs with high drug-loading efficiencies and payloads. The DOX-loading efficiency reached up to 9.1 wt% in MIL-100; the azidothymidine-triphosphate-loading efficiency in MIL-89, MIL-100 and MIL-53 were 0.6, 21.2 and 0.24 wt%, respectively; the cidofovir-loading efficiency in MIL-89, MIL-88A and MIL-100 were 14, 2.6 and 16.1 wt%. The release tests showed that there was no 'burst effect' for the three drug compounds in the MIL-100 nanoparticles because the release process was mainly governed by diffusion from the pore and drug/matrix interaction. These materials also demonstrated negligible toxicity in *in vivo* studies, indicating the good biocompatibility.

When it comes to nanomedicine applications, both functionality and biocompatibility of the nanomaterial must be considered [30]. Rosi and colleagues reported the cation-triggered drug release of procainamide HCl with Zinc-Adenine MOFs (denoted as bio-MOF-1), which was constructed from adenine molecules and zinc acetate [30]. The procainamide HCl drug-loading efficiency of bio-MOF-1 reached 0.22 g/g. The procainamide HCl release from the bio-MOF-1 was monitored in 0.1 M phosphate-buffered saline (PBS) solution (pH 7.4). A steady release was observed over 20 h with complete release achieved after 72 h. The bio-MOF-1 maintained its integrity throughout the release process. Wang and colleagues constructed the chiral nanoporous MOFs in dimethylformamide/methanol mixture solution by using the hexadentate ligand 5,5′,5′-(1,3,5-triazine-2,4,6-triyl)tris(azanediyl) triisophthalate and zinc ions [31]. After loading with anticancer drug 5-fluorouracil (5-FU), the MOFs still maintained their crystal structures and showed a maximal drug-loading efficiency of 0.5 g/g. The high loading capability was attributed to hydrogen bonding between the carbonyl group of 5-FU and the amine group in the MOF structure. The drug release was tested in PBS solution (pH 7.4) at room temperature. No 'burst effect' was observed and the release profile demonstrated three different release stages, corresponding to the different sizes of nanoscale cages (there have two different sized nanocages 6.3 × 10.5 Å and 14.3 × 11.5 Å in the MOF materials) and interactions. Later, the same group studied the zeolitic imidazolate framework-8 (ZIF-8; constructed by 2-methylimidazole and Zn^{2+}) as the potential drug carrier for 5-FU [32]. It was found that the ZIF-8 exhibited a higher capacity for the 5-FU (0.66 g/g). In the release experiments, the drug released much faster in mild acidic buffer solution (pH 5.0) than

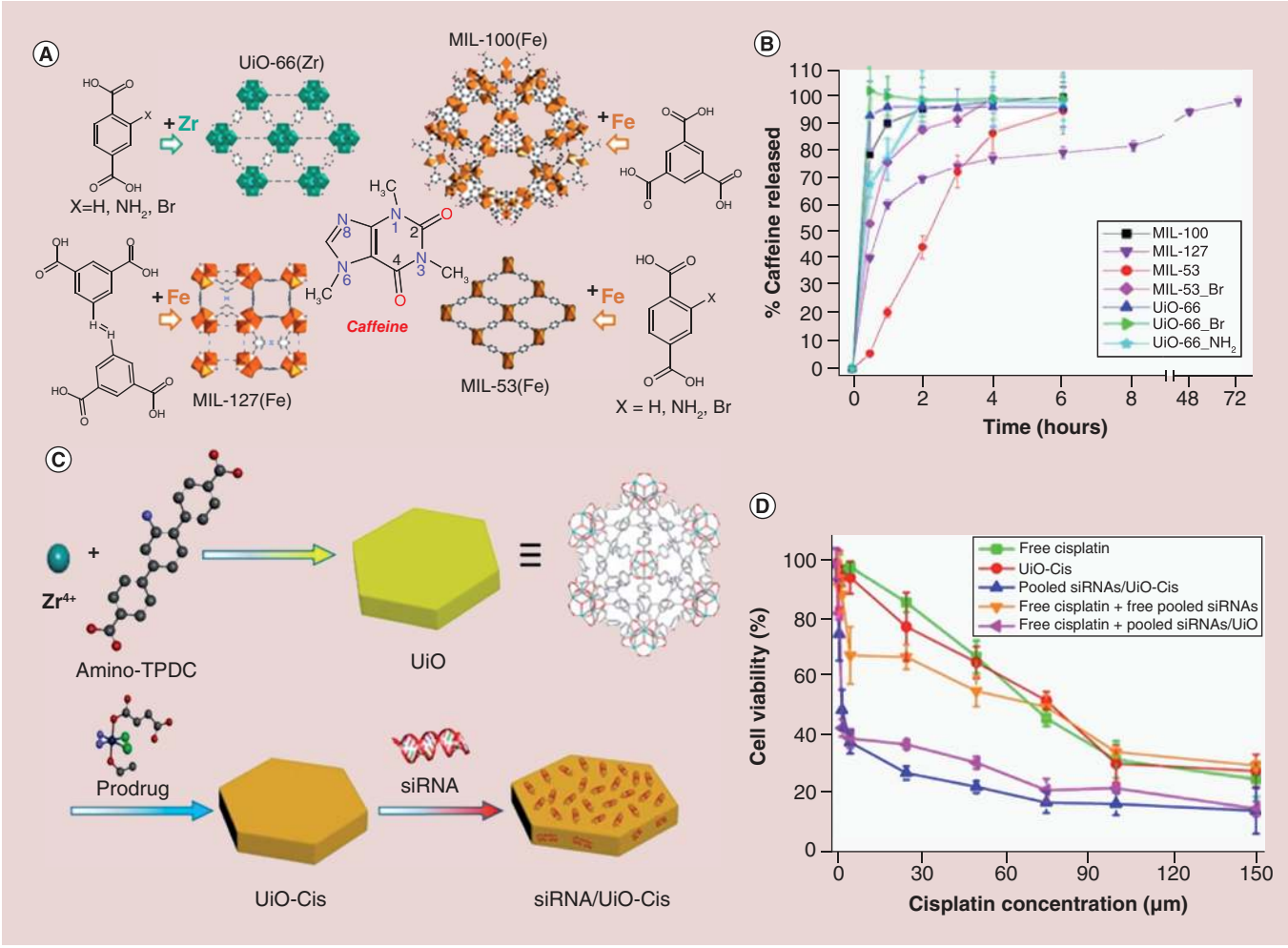

Figure 1. The nanoscale metal-organic frameworks as drugs and genes carriers. (A) The structures of MIL-100, UiO-66, MIL-127 and MIL-53 and caffeine molecule. **(B)** Caffeine release profiles from different porous metal-organic frameworks in PBS solution at 37°C. **(C)** Schematic presentation of *siRNA*/UiO-cisplatin synthesis and prodrug loading. **(D)** Cytotoxicity results of the SKOV-3 cells incubated with different samples showing the resensitization effect with *siRNA*/UiO-cisplatin nanoparticles.
MIL: Materials of Institute Lavoisier; UiO: Universitetet i Oslo.
(A) Reproduced with permission from [33] © American Chemical Society (2013).
(B) Reproduced with permission from [33] © American Chemical Society (2013).
(C) Reproduced with permission from [34] © American Chemical Society licensed with Standard ACS Author Choice/Editors' Choice usage agreement (2014).
(D) Reproduced with permission from [34] © American Chemical Society licensed with Standard ACS Author Choice/Editors' Choice usage agreement (2014).
For further permissions, please contact the ACS here: http://pubs.acs.org/copyright/permissions.html.

that in the neutral buffer solution. The faster drug release was ascribed to the dissolution property of the ZIF-8 structure in acidic conditions.

Recently, Serre and colleagues studied systematically the driving forces that governed the encapsulation of caffeine and the kinetics of drug delivery using four kinds of porous MOFs (MIL-100 [Fe], MIL-127 [Fe], MIL-53 [Fe] and UiO-66 [Zr]; UiO: Universitetet i Oslo) with different topology structures and chemical compositions (Figure 1A) [33]. The drug-loading tests showed that the caffeine-entrapping payload reached 49.5% in MIL-100, while only 22.4, 29.2 and 15.9% were observed for UiO-66, MIL-53 and MIL-127, respectively. The higher payload was due to the high surface area and the larger pore structures of MIL-100. The release profiles of the caffeine were dependent on the stability of the MOFs, caffeine mobility and the MOF-caffeine interactions. A 'burst effect' was observed as about 79 and 93% caffeine was released from MIL-100 and UiO-66 in the first 30 min (Figure 1B). While around 53, 68, 100% of caffeine was released in the first 30 min from the MIL-53-Br, UiO-

66-NH_2 and UiO-66-Br, respectively. The observed 'burst effect' was attributed to the collapse of Zr-based MOF (UiO-66-NH_2 and UiO-66-Br) in PBS solution due to the stronger binding affinity between Zr and phosphate ions. The excess phosphate ions in buffer decomposed the Zr-based MOFs quickly, leading to the immediate release of caffeine. In formulations where caffeine release was slower, it was hypothesized that the caffeine molecules interacted with the surface of the pore walls via van der Waals or π–π interactions.

Multidrug loading can significantly enhance cancer therapeutic efficacy. Lin and colleagues reported the codelivery of cisplatin and multiple drug resistance gene-silencing *siRNA* with hexagonal-plate like UiO MOFs (constructed by $ZrCl_4$ and amino-triphenyldicarboxylic acid; Figure 1C) [34]. In this work, the small-molecular prodrug cisplatin was encapsulated into the porous UiO MOFs via noncovalent interactions with a loading efficiency of 12.3%. The *siRNA* was then loaded by mixing the UiO-cisplatin complex with the *siRNA* aqueous solution. A much higher *siRNA*-loading efficiency was achieved (81.6%). Rather than loading into the pores of UiO MOFs, *siRNA* was conjugated onto the surface of MOFs through the coordination between the phosphate backbone of *siRNA* and surface Zr nodes. The transmission electron microscopy (TEM) images showed that Zr-triphenyldicarboxylic acid had a plate shape with approximately 100 nm in diameter and approximately 30 nm in thickness. With this multidrug-loading strategy using the UiO MOFs, the IC_{50} of the *siRNA*-loaded UiO-cisplatin (4.7) decreased dramatically compared with that of UiO-cisplatin (53.2) and free cisplatin (53.9), an order of magnitude enhancement in chemotherapeutic efficacy toward cisplatin-resistant ovarian cancer model was achieved (Figure 1D). Engelke and colleagues also investigated the codelivery of multiple drugs from MOFs. In their work, the irinotecan and floxuridine were successfully loaded into the MIL-88A, then the drugs-loaded MIL-88A was coated with DOPC (1,2-dioleoyl-*sn*-glycero-3-phosphocholine)-derived liposomes, which demonstrated no premature leakage [35].

Due to weak coordination binding between the metal ion and organic ligand, some MOFs may not be very stable in acid solutions [36]. However, acid-resistant MOFs are necessary for transporting drugs through an acidic environment like the stomach. Farha and colleagues developed an acid-resistant mesoporous NU-1000 (Zr-based MOFs) for oral insulin delivery [37]. Insulin was encapsulated into NU-1000 crystals by simple physical adsorption at room temperature, with a reported loading capacity of 40% [37]. More importantly, the NU-1000 had a suitable mesopore size of 31 × 13 Å. This allowed the encapsulation of insulin that has a molecular diameter of approximately 2.7 nm, [38] and prevented pepsin (48 × 64 Å) from entering and metabolizing the insulin. When exposed to simulated blood solution that has a high concentration of phosphate ions, the NU-1000 undergoes slow degradation to release insulin gradually. Another elegant design of insulin delivery was achieved using acid-responsive ZIF-8 nanoparticles, in which glucose oxidase and insulin were loaded. In high glucose concentration environment, glucose will be oxidized by glucose oxidase to gluconic acid, which subsequently decomposes ZIF-8 to release insulin [36,39].

Teplensky *et al.* loaded calcein and α-cyano-4-hydroxycinnamic acid into NU-1000 and NU-901, which are two Zr-based MOFs that have a high level of biocompatibility [40]. Due to the large pore sizes for NU-1000 and NU-901 (31 and 27 Å), both NU-1000 and NU-901 were treated with high temperature calcination (180°C) after calcein loading in order to obtain partial pore collapse and entrap the calcein to achieve a controlled release. The release tests were carried out with both native and calcination treated samples. In the first 4 h, 28, 10, 21 and 16% of calcein release for native NU-1000, calcination treated NU-1000, native NU-901 and calcination treated NU901, respectively, were observed. Slower release rate from calcination-treated MOFs suggested that the calcination treatment on MOFs can be used to control the release rate. Structured illumination microscopy was used to visualize the cellular uptake of MOFs. It was found that both the crystalline and treated MOFs (with and without drug loading) could be taken up by the HeLa cells, and that the MOFs moved much faster in the extracellular space than within the cells due to the medium differences.

The postencapsulation method is relatively simple for drug loading (especially for hydrophobic drugs); however, it also has drawbacks. For example, the drugs can be released at the undesired locations due to the uniform porous structure. On the other hand, the pH- or phosphate-responsive stability issues may also cause premature drug release before the nanoparticle reaches its intended target. Consequently, improving the stability of MOF nanostructures is crucial for MOF-based applications.

Drug loading with *in situ* encapsulation method

The postencapsulation methods have been widely used for drug loading in porous MOF materials. The two-step encapsulation method is relatively time-consuming and it remains limited by issues like premature drug release. Also, only drugs with a diameter smaller than the MOF channel can be loaded into porous MOFs. To solve this

problem, methods such as *in situ* drug encapsulation was explored recently. For example, Morsali and colleagues developed a procedure for the *in situ* synthesis of drug loaded $Zn_2(1,4\text{-bdc})_2(dabco)$ (bdc: 1,4-benzenedicarboxylic acid, dabco: 1,4-diazabicyclo[2.2.2]octane) MOFs at room temperature [41]. The drug IBU dissolved in hexane was mixed with $Zn_2(1,4\text{-bdc})_2(dabco)$ precursors under stirring for IBU loading. The IBU-loaded MOF complex was studied and 15% loading efficiency was reached with 72 h stirring. Although a burst effect was observed in the first few hours, the release rate decreased thereafter and about 80% of the drug was released gradually over 12 days. The two different release periods were explained by two different release mechanisms: the simple diffusion of the weakly bonded IBU for the first burst effect period and the stronger interactions between the MOFs and IBU for the second release period.

ZIF-8 is another widely used drug carrier for *in situ*-encapsulating drug molecules, due to its facile synthesis at room temperature, tunable size, porous structure, low cytotoxicity and biodegradable [42]. Tsung and colleagues developed a general synthetic route to encapsulate *in situ* small molecules into monodisperse 70-nm ZIF-8 nanospheres for controlled drug delivery (Figure 2A) [42]. Small molecules such as fluorescein and anticancer drug camptothecin (CPT) were successfully encapsulated into ZIF-8 framework structures by simply mixing the ZIF-8 precursors zinc nitrate and 2-methylimidazole in the presence of fluorescein and CPT in methanol. ZIF-8 is very stable in aqueous solution and it possesses a pore size of 11.6 Å in diameter, which connected through a small window (3.4 Å) [43]. Once encapsulated into ZIF-8 frameworks during the synthesis, the cargos remain embedded in the framework until the decomposition of the MOFs. In their studies, the maximal fluorescein and CPT-loading amounts were 1 and 2%, respectively. The drug release experiments showed that the ZIF-8 maintained its structures in neutral PBS solution, but dissociated in the pH 6.0 solution. This was also confirmed by TEM images. The release profiles revealed that less than 10% of the encapsulated fluorescein was released within 24 h in a neutral environment, while as high as 50% of the encapsulated fluorescein was released in 1 h upon exposure to an acidic buffer solution (Figure 2B). The *in vitro* studies showed the CPT-loaded ZIF-8 had a much better tumoricidal effect than that of the free CPT in MCF-7 cancer cells (Figure 2C). Subsequently, the same group successfully encapsulated a larger sized catalase enzyme (~10 nm) into ZIF-90 nanoparticles with a 5% loading capacity through an *in situ* encapsulation method [44], despite the fact that the ZIF-90 only has a small microporous size of 11.2 Å in diameter and an aperture size of 3.5 Å (Figure 2F) [45]. SDS-PAGE and confocal images further confirmed successful catalase encapsulation in the ZIF-90 nanostructures (Figure 2G & H). These tests demonstrated the advantages of the one-pot *in situ* drug/cargo encapsulation method over the two-step postencapsulation method, which was severely limited by the pore/channel size of the MOF materials. Alsaiari *et al.* reported that *CRISPR/Cas9* could be successfully encapsulated into nanoscale ZIF-8 (constructed by 2-methylimidazole and Zn^{2+}) with a loading efficiency of 17% by using an *in situ* method despite the relatively large size of *CRISPR/Cas9* [46].

Adopting a similar *in situ* encapsulation method, Zou and colleagues successfully obtained DOX, rhodamine B, methyl orange and methylene blue-encapsulated ZIF-8 nanocrystals using a one-pot approach (Figure 2D) [47]. Different from normal ZIF-8 nanoparticles, the TEM images showed that 5–15-nm-sized mesopores homogeneously distributed within the ZIF-8 crystals, especially in the high DOX-loading case (Figure 2E). Interestingly, the mesoporous structures only appeared in the inner part of ZIF-8 and no mesopores were observed in the outer shell that was approximately 20 nm in thickness (Figure 2E). This was mainly attributed to the depletion of target molecules. Notably, the mesoporous-free shell protected the encapsulated drug from premature release, and the inner mesoporous structure could provide adequate room to load drugs of larger sizes. By changing the reaction conditions, the DOX-loading efficiency reached 20% suggesting that ZIF-8 was an efficient drug delivery vehicle. This *in situ* DOX encapsulation using ZIF-8 as a carrier could store DOX safely in ZIF-8 with negligible release in PBS solution (pH 7.4) for 7 days at 60°C. Rather than loading the drugs into the intrinsic meso-/microporous structures (such as MIL-100 [Fe]), which may cause premature and uncontrollable drug release, ZIF-8 capped the drugs through a cooperation strategy [48]. Furthermore, the unique structure of ZIF-8 made it a pH-responsive drug release carrier. The loaded drugs remained in the ZIF-8 carriers during circulation and was released at the tumor sites, where the acidic environment disrupts the coordination interactions between imidazolate and zinc resulting in a rapid drug release. Alternatively, Chulkaivalsucharit *et al.* reported a reverse micelle method to *in situ* encapsulate the enzyme horseradish peroxidase (HRP) [49]. In this work, reverse micelle solution containing Zn^{2+} in a mixture of Brij C10, cyclohexane and water was mixed with 2-methylimidazole and HRP reverse micelle solution. The as-prepared HRP-encapsulated ZIF-8 had an average size of 30 nm where the incorporated HRP had a two- to fivefold higher activity than free HRP in solution. The *in situ* encapsulation method provided the possibility for loading/encapsulating of molecules that are larger than that of MOF intrinsic channels or pores.

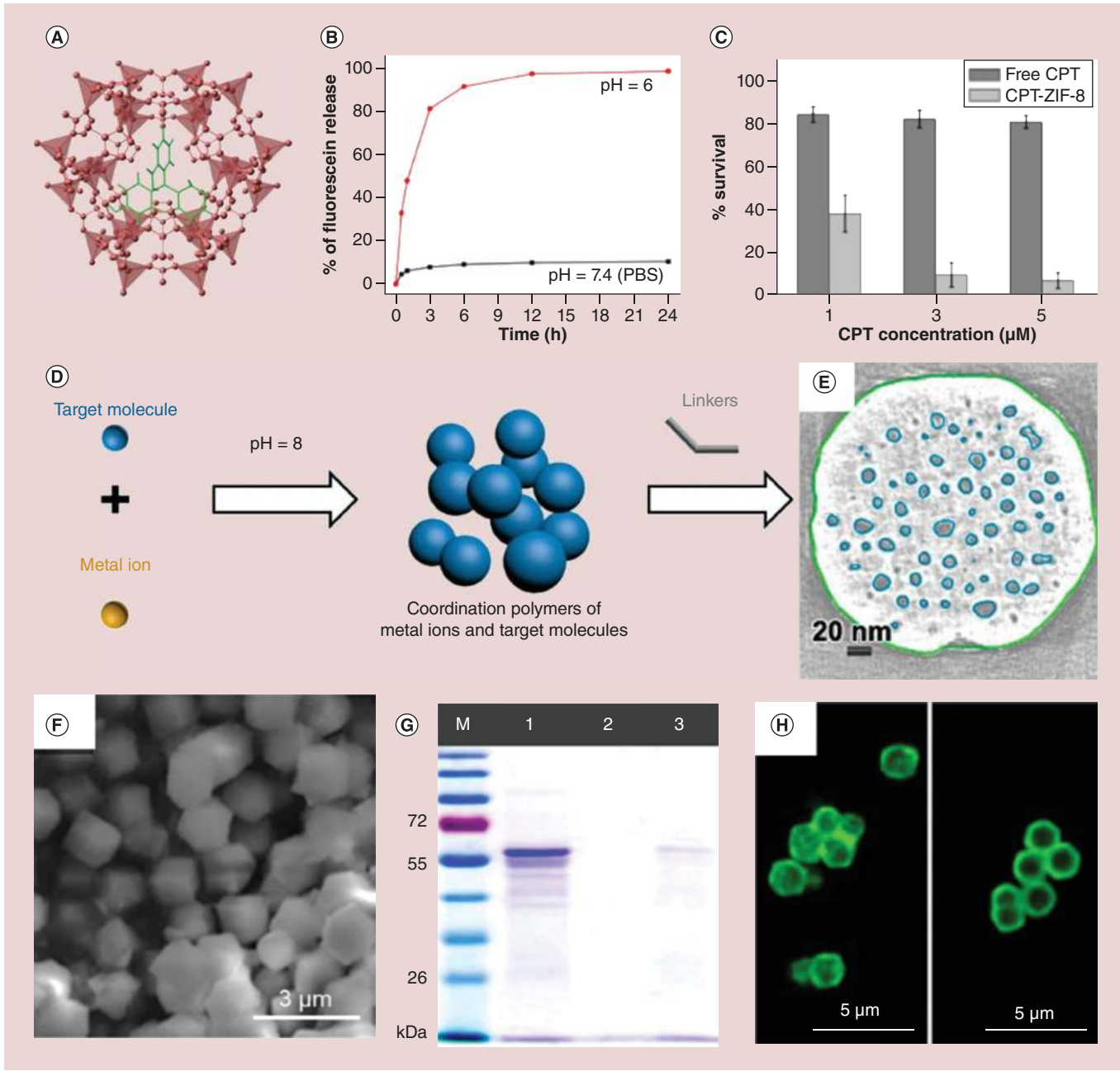

Figure 2. ***In situ*** **encapsulating drug molecules into nanoscale metal-organic frameworks. (A)** Topological structure of the fluorescein-loaded ZIF-8 framework. **(B)** pH-responsive fluorescein release profiles in PBS solution. **(C)** Cell viability of MCF-7 cells incubated with free CPT and CPT loaded ZIF-8 nanoparticles. **(D)** pH-induced *in situ* synthesis of drug-loaded zeolitic imidazolate framework-8 (ZIF-8) nanoparticles. **(E)** Cross-section of the electron tomogram of mesoporous structure distribution in the doxorubicin-loaded ZIF-8 nanoparticles. **(F)** Scanning electron microscope image of catalase-loaded ZIF-90 nanoparticles. **(G)** SDS-PAGE gel image (M: protein marker, lane 1: free catalase, lane 2: washed ZIF-90 with catalase on the surface, lane 3: catalase-loaded ZIF-90). **(H)** Confocal microscopy images of fluorescently (FITC)-labeled catalase-loaded ZIF-90 sample (left) and ZIF-90 with fluorescein isothiocyanate-catalase on its surface (right).
CPT: Camptothecin; ZIF-8: Zeolitic imidazolate framework-8.
(A) Reproduced with permission from [42] © American Chemical Society (2014).
(B) Reproduced with permission from [42] © American Chemical Society (2014).
(C) Reproduced with permission from [42] © American Chemical Society (2014).
(D) Reproduced with permission from [47] © American Chemical Society (2016).
(E) Reproduced with permission from [47] © American Chemical Society (2016).
(F) Reproduced with permission from [44] © American Chemical Society (2015).
(G) Reproduced with permission from [44] © American Chemical Society (2015).
(H) Reproduced with permission from [44] © American Chemical Society (2015).

This method not only prevented the leakage of loaded drug/cargo but also expanded the selection of the MOFs for different drug/cargo molecules. Notably, the *in situ* encapsulation method was widely extended to other kinds of MOF-based hybrid functional materials, such as DOX [47], biomolecules [50–53], inorganic nanoparticles [54–56] and quantum dots [57]. However, so far only very few kinds of MOF nanomaterials can use this *in situ* drug encapsulation method.

Functional MOF nanocompositions for drug delivery

The application of nanomaterials depends on surface property, shape, size and composition of the nanomaterials. MOF is an interesting class of nanomaterials because of its tunable shape and size, and surface functionalities. MOFs of different sizes or morphologies can be easily obtained by changing the reaction conditions [58–60]. Moreover, the surface of the MOFs can be modified and functionalized with biomolecules or polymers to provide stability, biocompatibility and/or functionality [61]. For example, the chemistry between the functional units and coordinatively unsaturated metal sites or prefunctionalized linkers on the external surface of MOFs could be used for different functionalizations [62–65]. With a careful control over the MOF host–guest interaction or coating the surface of MOFs with a thin layer of silica, responsive polymer or lipid bilayer is an alternative way to improve the stability and biocompatibility of the MOF carriers [25,29,61,66–69]. After surface modification or surface coating, the MOFs may obtain a stimuli-responsive drug release property due to the functionalized ligands or coating layers.

pH-responsive drug release

Lin and colleagues described a general method to coat rare-earth cations based-fluorescent nanoscale MOFs (constructed by Eu^{3+}, Gd^{3+}, Tb^{3+} and 1,4-benzenedicarboxylate) with silica layers (Figure 3A) [61]. The as-prepared nanoscale MOFs were first treated with polyvinylpyrrolidone by simply mixing, and subsequently coated with silica of different thicknesses using a sol-gel procedure. The outer silica layer stabilized the nanoscale MOF cores against dissolution at different pH environment (Figure 3B & C). These kinds of core-shell nanomaterials can be used for controlled drug release. In another work, the Lin group introduced amino groups into the MOF frameworks by doping the terephthalic acid (the ligand) with 2-aminoterephthalic acid during the synthesis of MIL-101 MOFs [70]. The anticancer prodrug cisplatin (ESCP: ethoxysuccinato-cisplatin) and the dye BODIPY (Br-BODIPY: 1,3,5,7-tetramethyl-4,4-di uoro-8-bromomethyl-4-bora-3a,4a-diaza-s-indacene) were attached to the MOF ligands through the amide and amine bonds (Figure 3D). The MOF nanoparticles were further coated with a thin layer of silica to enhance the stability in biological conditions (Figure 3E) [70]. The silica-coated MIL-101 (Fe) slowed the cargo release and greatly increased their physical half-life in PBS buffer at 37°C compared with ESCP-conjugated MIL-101 (Fe) without silica coating (Figure 3F). After functionalization with a cyclic peptide targeting $\alpha_v\beta_3$ integrin, the cisplatin prodrug loaded MIL-101 (Fe) showed better cytotoxicity than that of cisplatin prodrug alone for HT29 human colorectal cancer cells. This work provided a new strategy for postsynthetic conjugation of nanoscale MOFs with anticancer drugs for simultaneous imaging and drug delivery.

Che and colleagues rationally designed core–shell coordination polymer-coated nanostructures for delivery of methotrexate (MTX) and S-(*N-p*-chloro-phenyl-N-hydroxycarbamoyl)glutathione (CHG) (Figure 3G & H) [71]. The inner core, which was constructed by Zn^{2+} or Fe^{3+} with MTX or CHG, was physiologically unstable. In their studies, the Zn-MTX, Fe-MTX and Fe-CHG nanoparticles showed sphere morphology with diameters of ~145, ~160 and ~155 nm, respectively. The coordination polymer synthesized from 1,4-bis(imidazole(1-ylmethyl) benzene) (BIX) and Zn^{2+} was then coated onto the surface of Zn-MTX, Fe-MTX and Fe-CHG nanospheres to form core–shell functional nanoparticles. In this core–shell nanostructure, the inner MOF cores acted as drug reservoirs and the coordination bond in the outer coordination polymer shell could be decomposed by a drop in external pH. This resulted in the decomposition of the shells and the exposure of the 'drug reservoirs' cores, leading to drug release (Figure 3I). The polymer shell coating increased the stability of the MOF, conferred pH-responsiveness properties and enhanced cytotoxicity toward HeLa cells.

In 2017, Forgan and colleagues reported a method that incorporated polymers onto the surface of nanoscale zirconium UiO-66 MOFs in order to enhance stability and drug delivery [72]. The UiO-66 nanoparticles constructed by 1,4-benzenedicarboxylate and $ZrCl_4$ were synthesized with the addition of desired modulators (*p*-azidomethylbenzoic acid [L1] and *p*-propargyloxybenzoic acid [L2]) and acetic acid. After that, the postsynthetic modification by azide-alkyne cycloaddition was carried out. Specifically, PEG chains (MW.2000 and MW.550) with alkylated propargyl units were conjugated onto azide-functionalized UiO-66 nanoparticles via click reaction. Simply mixing the azide-UiO-66 with a concentrated calcein methanolic solution resulted in a calcein-loaded

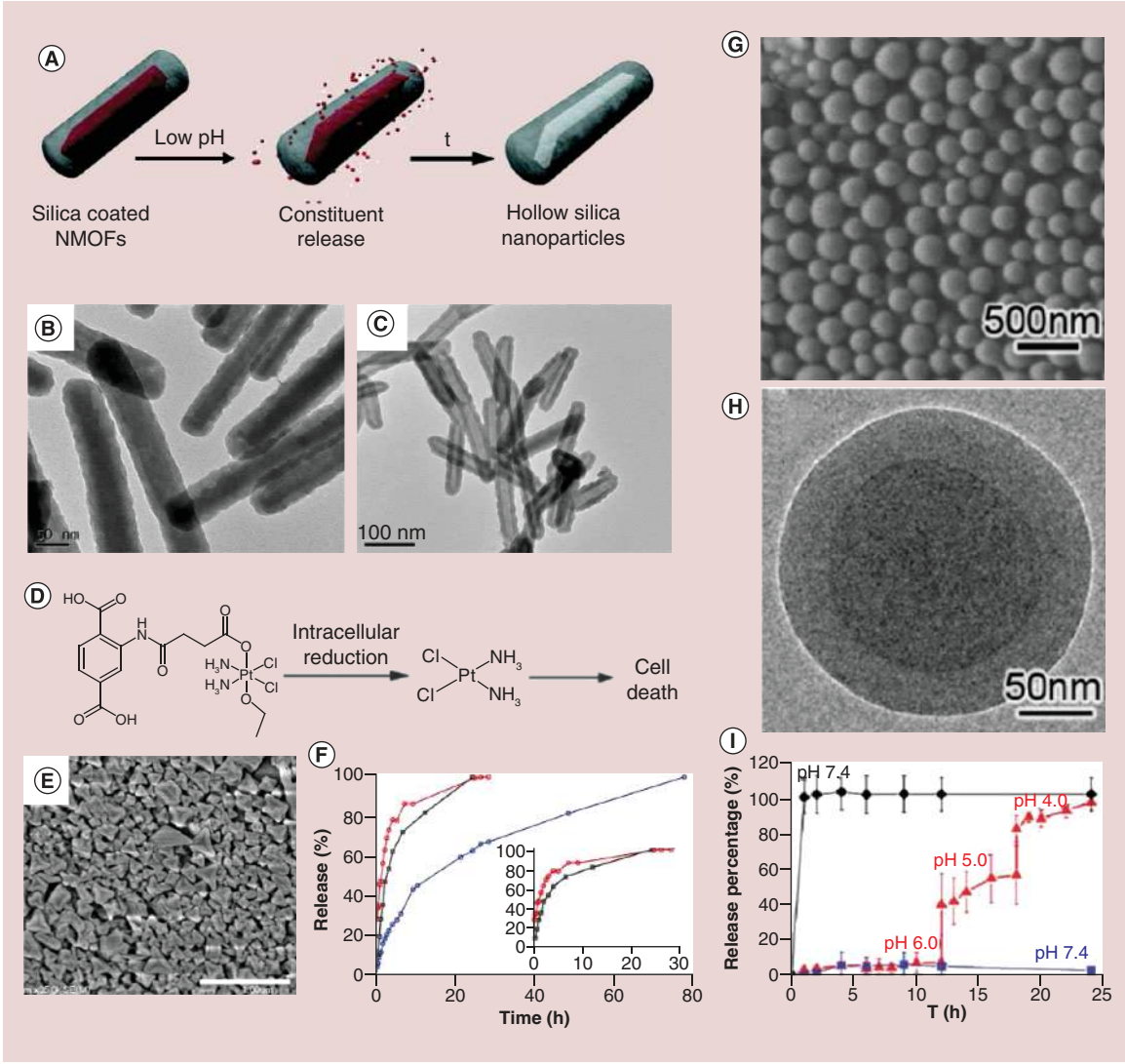

Figure 3. Functional metal-organic framework nanocompositions for pH-responsive drug release. (A) Scheme of pH-responsive drug release from the rare-earth cations (Eu, Gd or Tb) MOF nanorods. **(B)** Transmission electron microscopy image of 8–9 nm silica layer-coated MOF nanorods before and **(C)** after cargo release at pH 4.0. **(D)** Structure of the prodrug of cisplatin ethoxysuccinato-cisplatin. **(E)** Scanning electron microscope image of silica-coating cisplatin-loaded Materials of Institute Lavoisier(MIL)-101 (Fe), scale bar 1 μm. **(F)** BDC-NH-BODIPY dye release profile (black line) from the BODIPY-loaded MIL-101 (Fe) in phosphate-buffered saline buffer, BDC-NH-ESCP release profiles from the ESCP-loaded MIL-101 (Fe; red line) and from the silica-coated ESCP-loaded MIL-101 (Fe; blue line) in phosphate-buffered saline buffer solutions. **(G)** Scanning electron microscope and **(H)** transmission electron microscopy images of methotrexate-Zn@1,4-Bis(imidazole(1-ylmethyl) benzene)-Zn. **(I)** Calcein release profiles of methotrexate-Zn (diamond) and methotrexate-Zn@1,4-Bis(imidazole(1-ylmethyl) benzene)-Zn (triangle, square) with stepwise acidification.
MOF: Metal-organic framework.
(A) Reproduced with permission from [61] © American Chemical Society (2007).
(B) Reproduced with permission from [61] © American Chemical Society (2007).
(C) Reproduced with permission from [61] © American Chemical Society (2007).
(D) Reproduced with permission from [70] © American Chemical Society (2009).
(E) Reproduced with permission from [70] © American Chemical Society (2009).
(F) Reproduced with permission from [70] © American Chemical Society (2009).
(G) & (H) Reproduced with permission from [71] © Royal Society of Chemistry (2012).
(I) Reproduced with permission from [71] © Royal Society of Chemistry (2012).

PEGylated UiO-66 nanocomplex with calcein load efficiency of 16.0%. Further studies showed that the calcein release was pH-responsive for both PEGylated and non-PEGylated samples. The surface modification effect on calcein release was then monitored in PBS solution at pH 5.5 and 7.4. As predicted, the samples with PEGylation showed slower calcein release at pH 7.4, with less than 30% of calcein released within 5 days, while a rapid release of calcein (80%) was observed within 1 h at pH 5.5 with near complete release after 2 days. The authors hypothesized that the phosphate in the PBS solution might attack the ligands on the surface of UiO-66 and replace the surface ligands. Without PEGylation, MOFs were more susceptible to be attacked leading to faster ligand exchange. At low pH, the carboxylate ligands are protonated resulting in faster MOF degradation and pH-responsive drug release.

Ion/small molecular-responsive drug release

Mirkin and colleagues functionalized the UiO-66-N_3 surface with nucleic acid (DNA) via click reaction for improving the stability and cellular uptake of the MOF materials [73]. In this work, they discovered that the DNA-conjugated UiO-66-N_3 exhibited increased stability in high salt solution compared with unfunctionalized MOF nanoparticles [73].

Alternately, Willner and colleagues reported the DNA functionalized stimuli-responsive nanoscale UiO-68 system for controlled drug release [74]. The DNA capping units were composed of pH-responsive DNA duplex units or metal–ion-responsive DNAzyme/substrate complexes. In the presence of the appropriate stimuli, encapsulated anticancer drugs within the UiO-68 nanoparticles were released. Specifically, amine-functionalized triphenyl carboxylic acid was reacted with $ZrCl_4$ to yield the UiO-68 nanoparticles. The obtained UiO-68 nanoparticles had a bipyramidal shape with a size of 250–300 nm. To attach the DNA sequences, the amine groups in the UiO-68 surface were converted to azide groups in the presence of *t*-butyl and trimethylsilyl azide. Through click reaction, the DNA sequences were conjugated onto the surface of DOX-loaded UiO-68 nanoparticles. Subsequently, the UiO-68 nanoparticles were capped with the complementary cytosine (C)-rich DNA sequences, which can reconfigure in the acidic environment into an i-motif structure to lock in the loaded DOX molecules. The *in vitro* tests showed that the DOX release from the DNA-modified UiO-68 nanoparticles was much faster at pH 5.0 than at pH 7.0, which could be attributed to the reconfiguration of the hybrid DNA duplex into a different i-motif structure that unlocked the duplex capping units and release of the loaded DOX.

The UiO-68 nanoparticles can also be capped with other ion-dependent (Mg^{2+}, Pb^{2+}) DNAzymes. In the presence of the target ions, the DNAzyme becomes activated and cleaves the capping units e releases the drugs [74]. In this design, a foreign sequence like an aptamer sequence (aptamer-ligand complex) can be used as the auxiliary trigger for the Mg^{2+} ion-dependent DNAzyme loop. For example, the smart ATP-responsive Mg^{2+} ion-dependent DNAzyme-capped DOX-loaded UiO-68 nanoparticles was utilized for treatment of cancer cells, where the Mg^{2+}-dependent DNAzyme was separated by an ATP-aptamer sequence [74]. In this system, Mg^{2+} ion-triggered release of DOX was low compared with APT-induced DOX release, due to the stabilization of the catalytic loop through the ATP-aptamer complex formation. Later, Chen *et al.* designed another ATP-responsive DNA-based hydrogel-coated MOFs for drug delivery [75]. Specifically, amine-functionalized triphenyl carboxylic acid was reacted with $ZrCl_4$ to yield the nanoscale UiO-68 nanoparticles (Figure 4A). After DOX loading, the DOX-loaded UiO-68 nanoparticles were coated with stimuli-responsive acrylamide/DNA hydrogel. The hydrogel was cross-linked by two polyacrylamide chains, which were modified with two nucleic acid hairpins. The DNA duplex-bridged polyacrylamide hydrogel includes the anti-ATP aptamer sequence in a caged configuration. In the presence of ATP, the cross-linking units were cleaved and resulted in the dissociation of the hydrogel and the release of the DOX (Figure 4B). The *in vitro* studies, much better performance was observed in the DOX-loaded hydrogel-coated UiO-68 nanoparticles-treated MDA-MB-231 cells compared with the cells treated with DOX-loaded UiO-68 nanoparticles gated by ATP-responsive duplex units (Figure 4C & D). These studies provided the framework for designing novel ion/small molecular-responsive drug release system.

He and colleagues constructed an intrinsic redox-responsive drug delivery system based on MOFs, which were assembled with 4,4′-dithiobisbenzoic acid (4,4′-DTBA) and iron, aluminum or zirconium ions (Figure 4E) [76]. The disulfide bond in the MOFs structure would be cleaved with the overexpressed glutathione (GSH) in cancer cells (Figure 4F). The curcumin (CCM)-loaded MOFs showed a faster release rate in the presence of GSH in PBS buffer solution. Furthermore, the *in vivo* studies were done with xenograft cervical tumor-bearing BALB/c nude mice, which were treated with the saline, free CCM and CCM-loaded MOF-Zr(DTBA) nanoparticles. The results displayed a gradual tumor volume increase in the saline and free CCM groups, while the there was little change in

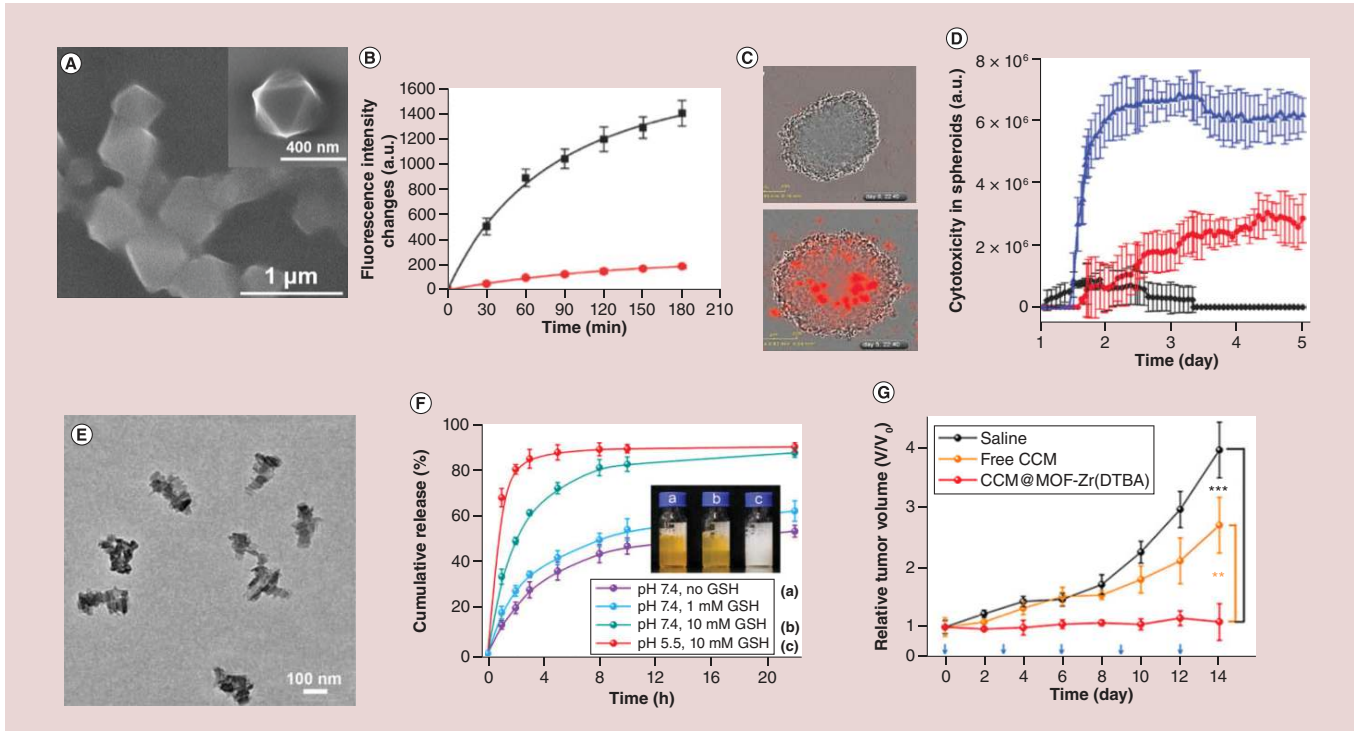

Figure 4. Functional metal-organic framework nanocompositions for stimuli-responsive drug release. (A) Scanning electron microscope image of a stimuli-responsive DNA-based polyacrylamide hydrogel-coated Universitetet i Oslo (UiO)-68 nanoparticles. **(B)** Release profiles of doxorubicin (DOX) from the hydrogel-coated UiO-68 nanoparticles upon addition of ATP (50×10^{-3} M, black line) and in absence of the ATP (red line). **(C)** Representative phase-contrast and red fluorescence images (indicative of the cell apoptosis) of the cell aggregates after time intervals of 24 h (top) and 120 h (down), where the cells were treated with DOX-loaded hydrogel-coated UiO-68 nanoparticles. **(D)** Apoptosis of the MDA-MB-231 cells treated with unloaded hydrogel-coated UiO-68 nanoparticles (black line), DOX-loaded UiO-68 nanoparticles gated by ATP-responsive duplex units (red line), and DOX-loaded ATP-responsive hydrogel-coated UiO-68 nanoparticles (blue line). **(E)** Transmission electron microscopy image of CCM@MOF-Zr (4,4′-DTBA) nanoparticles. **(F)** Glutathione-responsive release profiles from CCM@MOF-Zr (4,4′-Dithiobisbenzoic acid) nanoparticles in pH 5.5 and pH 7.4 phosphate-buffered saline solution. **(G)** Relative tumor volume and body weight of the mice.
CCM: Curcumin; DTBA: Dithiobisbenzoic acid; MOF: Metal-organic framework.
(A) Reproduced with permission from [75] © WILEY-VCH Verlag GmbH & Co. KGaA, Weinheim (2016).
(B) Reproduced with permission from [75] © WILEY-VCH Verlag GmbH & Co. KGaA, Weinheim (2016).
(C) Reproduced with permission from [75] © WILEY-VCH Verlag GmbH & Co. KGaA, Weinheim (2016).
(D) Reproduced with permission from [75] © WILEY-VCH Verlag GmbH & Co. KGaA, Weinheim (2016).
(E) Reproduced with permission from [76] © American Chemical Society (2018).
(F) Reproduced with permission from [76] © American Chemical Society (2018).
(G) Reproduced with permission from [76] © American Chemical Society (2018).

the tumor volume in 14 days from the CCM-loaded MOF-Zr(DTBA) group, displayed a higher therapy efficacy (Figure 4G).

Multistimuli-responsive drug release

Postsynthetic modification is another good option to achieve additional functionalities for controlled drug release for MOF materials. For example, Zhang and colleagues developed a MIL-101-N_3 (Fe)-based multifunctional and biocompatible drug delivery system, which showed enhanced cellular uptake and low pH-responsive drug release (Figure 5A) [66]. The MIL-101 (Fe) with azide moieties was first loaded with DOX, and subsequently modified with a bicyclononyne-functionalized β-cyclodextrin derivative (β-CD-SS-BCN) through strain-promoted [3+2] azide-alkyne cycloaddition (copper-free click reaction; Figure 5A). The β-CD-SS-BCN-modified MIL-101 (Fe) was then further functionalized with the αvβ3 integrin-targeting peptide polymer Lys(adamantane)-Arg-Gly-Asp-Ser-bi-PEG1900 (K(ad)RGDS-PEG1900, bi = benzoic imine) through the host–guest interaction (Figure 5A). In this structure, two stimuli-responsive triggers were achieved. The disulfide bond between the β-CD and the MIL-101 (Fe) can be oxidized by GSH, which can be found in high concentrations in cancer cells. For example,

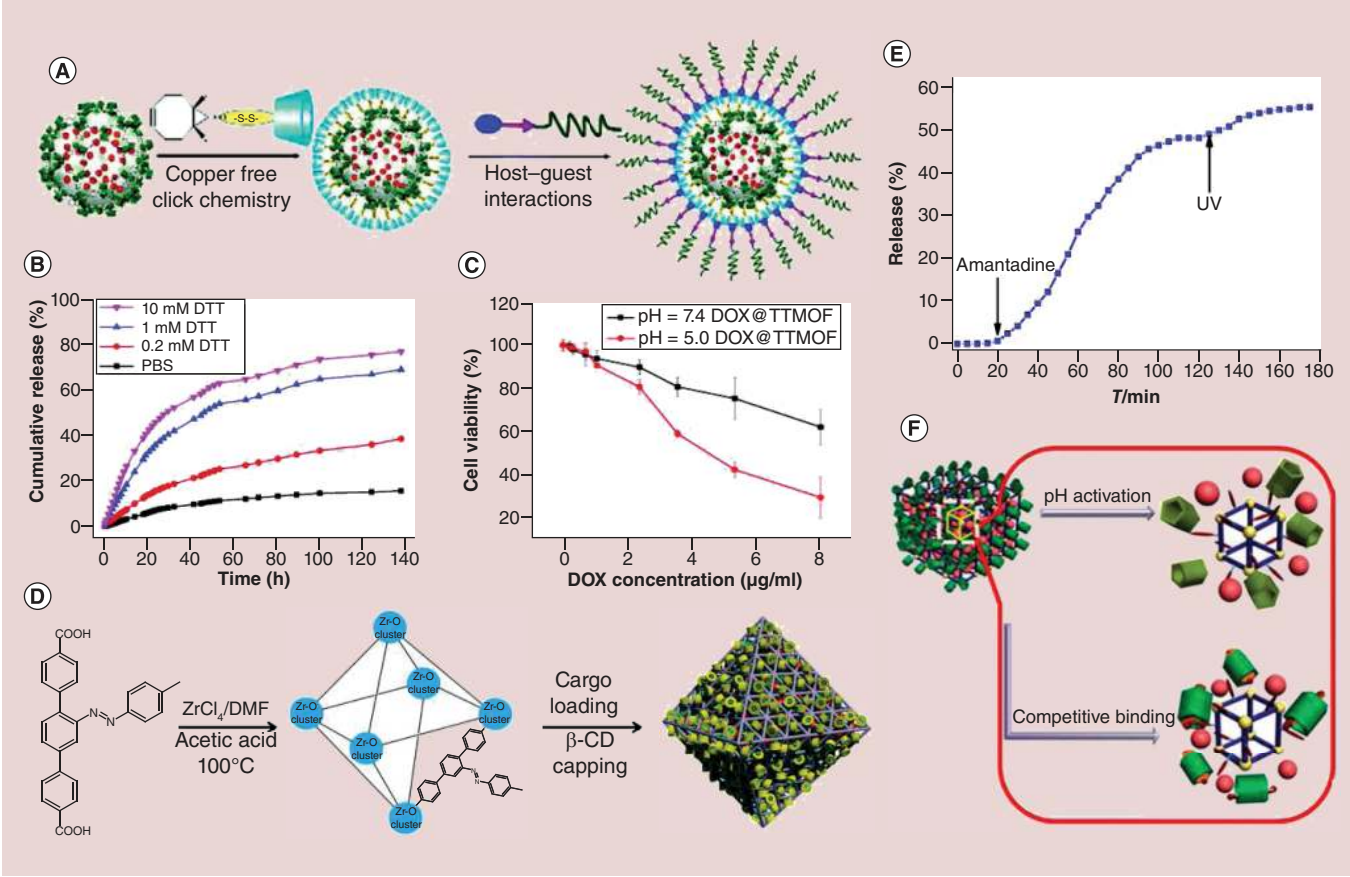

Figure 5. (A) Functional MOF nanocompositions for multistimuli-responsive drug release. Schematic of drug-loading and postsynthetic modification of the Materials of Institute Lavoisier (MIL)-101 (Fe). **(B)** DTT-responsive DOX release profiles from DOX-loaded targeting MIL-101 (Fe) in phosphate-buffered saline at various DTT concentrations. **(C)** Cell viability of the HeLa cells after treated with DOX-loaded targeting MIL-101 (Fe) at pH 5.0 and 7.4. **(D)** Illustration of the synthesis of cargo-loaded, β-CD-capped Universitetet i Oslo (UiO)-68-azo with azobenzene as stalks encircled by β-CD. **(E)** Release profiles of cargo-loaded, β-CD-capped UiO-68-azo in the presence of amantadine and UV irradiation. **(F)** Schematic of pH or competitive binding-responsive University of Michigan Crystalline Material-1-NH2 nanocarriers with positively charged pyridinium units (Py) as stalks encircled by pillarenes on the surfaces.
β-CD: β-cyclodextrin; DOX: Doxorubicin; DTT: Dithiothreitol; MOF: Metal-organic framework.
(A) Reproduced with permission from [66] © Royal Society of Chemistry (2015).
(B) Reproduced with permission from [66] © Royal Society of Chemistry (2015).
(C) Reproduced with permission from [66] © Royal Society of Chemistry (2015).
(D) Reproduced with permission from [77] © The Authors, some rights reserved; exclusive licensee American Association for the Advancement of Science (2016). Distributed under a Creative Commons Attribution NonCommercial License 4.0 (CC BY-NC) http://creativecommons.org/licenses/by-nc/4.0/.
(E) Reproduced with permission from [77] © The Authors, some rights reserved; exclusive licensee American Association for the Advancement of Science (2016). Distributed under a Creative Commons Attribution NonCommercial License 4.0 (CC BY-NC) https://creativecommons.org/licenses/by-nc/4.0/.
(F) Reproduced with permission from [67] © Royal Society of Chemistry licensed under a Creative Commons Attribution-NonCommercial 3.0 Unported Licence (2015).
For further permissions, please contact AAAS: http://www.sciencemag.org/help/reprints-and-permissions; and Royal Society of Chemistry: http://www.rsc.org/journals-books-databases/journal-authors-reviewers/licences-copyright-permissions/#deposition-sharing

the disulfide linker can also be cleaved by using reducing agents such as dithiothreitol (DTT; Figure 5B). On the other hand, the pH-responsive benzoic-imine bond between the poly(ethylene glycol) (PEG) and the targeting K(ad)RGDS peptide, which would be cleaved in the acidic tumor microenvironment (Figure 5C). The *in vitro* experimental results showed that the DOX release was highly depended on the reductant concentrations and the cytotoxicity of loaded DOX to normal cells was significantly reduced because of the surface modification. The *in vivo* studies showed the well-modified MIL-101 (Fe) could inhibit hepatoma H22 tumor progression effectively with minimal side effects.

Wang and colleagues reported a light-responsive UiO-68 nanoparticle for on-command cargo release (Figure 5D) [77]. In their studies, light-responsive release or competitive binding agent-responsive release systems were achieved by conjugation of β-cyclodextrin (β-CD) with the azobenzene-modified UiO-68 nanoparticles (β-CD capped UiO-68-azo). The azobenzene groups underwent photo-activated *cis*/*trans* isomerization to force the β-CD rings away, resulting the opening of the gates and release of the cargo (Figure 5E). The dissociation of the gatekeeper β-CD from the azobenzene can also be triggered by a competitive binding agent such as amantadine, which has a higher binding affinity to β-CD than azobenzene. The surface bioconjugation made the MOF platform very promising in the controlled drug delivery system.

The Yang group developed pH- and/or competitive binding triggered drug release system with miminal premature release [67]. The stimuli-responsive platform was based on the mechanized monodisperse UMCM-1-NH_2 (University of Michigan Crystalline Material [UMCM]) particles gated by carboxylatopillar [5] arene (CP5) switches (Figure 5F). The cargo was encapsulated via the CP5-pyridinium stalks host–guest complexation to form fluid mechanized [2] pseudorotaxanes nanocarriers. When methyl viologen salts were added, the supramolecular nanovalves opened and the cargo was released due to the high affinity attraction between methyl viologen and CP5. The rate of cargo release increased when more methyl viologen was added to the system. When subjected to low pH, the noncovalent bonding between the CP5-pyridinium stalks of the CP5 [2] pseudorotaxanes was weakened, resulting in the opening of the nanopores and further drug release. Given the low pH environment at the tumor sites, this system has the potential to be a controllable drug delivery platform for cancer therapy. Following this work, other research groups reported MOF-based ion/thermal-responsive [78] and ion/pH/thermal-responsive [79] drug release systems.

In recent decades, inorganic nanomaterials such as magnetic nanoparticles [80–83], plasmon noble metal nanomaterials [84–86] and other optical nanomaterials [87–89] have been widely used for theranostics due to their unique physical and chemical properties. The integration of external-functionalized nanomaterials into the MOF matrix can impart the additional properties to the MOF materials. Compared with the individual MOF platform, the integrated MOF-based hybrid multifunctional platforms not only maintain the porous property of MOFs but also gain intrinsic properties originating from the conjugated guest nanoparticles (e.g., Fe_3O_4, Au nanorods, upconversion nanoparticles). For example, Ke *et al.* fabricated $Fe_3O_4/Cu_3(BTC)_2$ (1,3,5-benzenetricarboxylic acid [BTC]) nanocomposites for targeted drug release systems [90]. The drug nimesulide was loaded in the magnetic nanocomposites by soaking $Fe_3O_4/Cu_3(BTC)_2$ in the nimesulide trichloromethane solution. A 16.7% of drug-loading capacity was achieved and complete drug release was observed after 11 days. The magnetic study suggested that $Fe_3O_4/Cu_3(BTC)_2$ nanocomposites exhibited desirable magnetic characteristics for targeted drug delivery. Similarly, Guan and colleagues reported a one-step synthesis to integrate γ-Fe_2O_3 into MIL-53 (Al) via pyrolysis of the magnetic ferric oxides precursors MOFs [91]. As expected, the γ-Fe_2O_3@MIL-53(Al) nanocomposites exhibited controlled drug release behavior in saline at 37°C. The loaded IBU was completely released after 7 days. Their experiments demonstrated that the magnetic γ-Fe_2O_3@MIL-53(Al) nanocomposites could be used for controlled drug delivery.

The presence of the iron ions or clusters within the MOFs enables their use as MRI contrast. For example, Chen and colleagues reported a multifunctional dual-imaging (MRI)-guided pH-responsive drug delivery system based on Fe_3O_4@carbon@ZIF-8 nanostructures (Figure 6A) [92]. The carbon-encapsulated Fe_3O_4 colloidal nanoparticles were first synthesized via the decomposition of ferrocene. Then, the ZIF-8 layer was grown on the surface of the negatively charged Fe_3O_4@carbon. In this multifunctional nanoplatform, the DOX-loading efficiency reached 42.2%, demonstrating a good maintenance of the porous structure. Due to the acid-sensitive nature of ZIF-8 shells, Fe_3O_4@carbon@ZIF-8 nanostructures could be easily used as a pH-responsive drug release system. Meanwhile, the spin–spin relaxation time (T_2^*)-weighted MRI evaluation showed that the Fe_3O_4@carbon@ZIF-8 nanostructures had good sensitivity as an MRI contrast agent for tumor diagnosis (Figure 6C). Additional *in vivo* experiments further demonstrated the high therapeutic efficacy of the DOX-loaded Fe_3O_4@carbon@ZIF-8 nanostructures (Figure 6D). The DOX-loaded Fe_3O_4@carbon@ZIF-8 nanostructures displayed the best performance in the inhibition of A549 lung cancer bearing mice than the PBS, free DOX and Fe_3O_4@carbon@ZIF-8 nanostructures groups (Figure 6D).

In 2017, Fu *et al.* fabricated core–shell Fe_3O_4@UiO-66 nanocomposites that were constructed through an *in situ* growth of UiO-66 shell on the surface of Fe_3O_4 nanoparticles (Figure 6E) [93]. For this nanocomposite, exceptionally high DOX-loading capacity (63%) and pH-responsive DOX release were achieved. At pH 4.0 and 5.0, around 36.1 and 21.6% DOX were released from the nanocomposites within 41 days, while only 17.1 and 13.8%

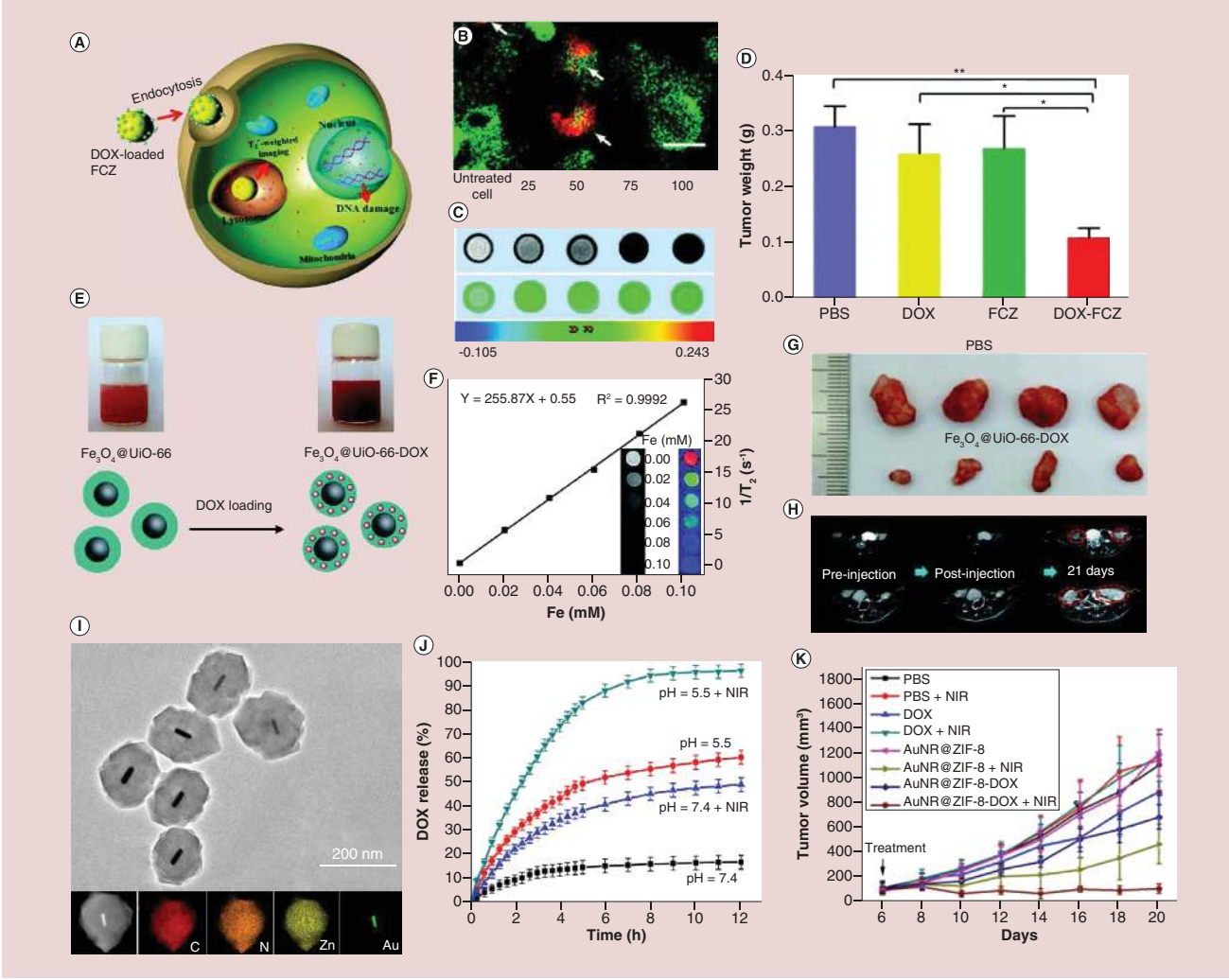

Figure 6. The application of functional metal-organic framework nanocompositions for theranostics. (A) Illustration of pH-responsive FCZ nanoparticles as drug delivery vehicles. **(B)** Subcellular localization of the FCZ nanoparticles by transfected HeLa cells with mecherry-LAMP-1. **(C)** T_2^*-weighted images of A549 cells with FCZ nanoparticles untreated and treated at different concentrations. **(D)** *In vivo* antitumor efficacy of DOX-loaded FCZ nanoparticles in the A549 lung cancer mice model tumor. **(E)** Scheme of the synthesis of DOX-loaded Fe_3O_4@UiO-66 core–shell nanoparticles for imaging and therapy. **(F)** T_2-weighted MRI images and transverse relativity of Fe_3O_4@UiO-66 at different Fe concentrations. **(G)** Tumor biopsies from the PBS and Fe_3O_4@UiO-66-DOX-treated mice on day 30. **(H)** MRI images of HeLa tumor-bearing mice treated by PBS and Fe_3O_4@UiO-66-DOX at different times. **(I)** Transmission electron microscopy image of the core–shell AuNR@ZIF-8 nanostructures, bottom: HAADF-STEM image and energy-dispersive X-ray spectroscopy elemental mapping of single AuNR@ZIF-8 core–shell nanoparticle. **(J)** DOX release profiles from the AuNR@ZIF-8-DOX nanostructures with and without 808-nm laser irradiation (1 w/cm^2) at different pH values. **(K)** Relative tumor volume from 4T1 tumor-bearing mice with different types of treatments.

DOX: Doxorubicin; FCZ: Fe3O4@C@ZIF-8; PBS: Phosphate-buffered saline; TEM: Transmission electron microscopy; UiO: Universitetet i Oslo; ZIF-8: Zeolitic imidazolate framework-8.

DOX were released at pH 6.0 and 7.4. The strong superparamagnetism of Fe_3O_4 endowed the Fe_3O_4@UiO-66 nanocomposites with the ability to act as a T_2 contrast agent for MRI (Figure 6F). The *in vitro* and *in vivo* toxicity studies showed that the Fe_3O_4@UiO-66 nanocomposites had good biocompatibility, sustained drug release and excellent MRI ability, as well as good therapeutic efficacy (Figure 6G & H). Similarly, Fe-based MIL-100 (Fe) multifunctional materials synthesized by the integration of rare-earth-doped upconversion nanoparticles have also been evaluated for multimodal image-guided drug delivery [95,96].

To combine the unique photothermal property of Au nanorods and the high drug-loading efficiency and pH-responsive dissociation of ZIF-8, Tang and colleagues prepared a core–shell AuNR@ZIF-8 nanostructure by mixing the AuNR@ZIF-8 nanostructures with DOX solution (Figure 6I). Under 808-nm laser irradiation, the AuNR@ZIF-8 core–shell nanostructures demonstrated notable photothermal effect, near-infrared (NIR) light and pH dual stimuli-responsive drug release (Figure 6J). The *in vivo* studies confirmed that the AuNR@ZIF-8-DOX nanostructures have higher toxicity for cells and 4T1 tumor xenografts compared with monotherapy with photothermal or chemotherapy therapy (Figure 6K). Under 808-nm laser irradiation, the AuNR@ZIF-8-DOX nanostructures injected mice exhibited the highest tumor inhibition (90%), in comparison to that of AuNR@ZIF-8-DOX nanostructures (30%, without NIR irradiation) and AuNR@ZIF-8 nanostructures (58%, with 808-nm laser irradiation), demonstrating notable synergistic effect of chemotherapy and photothermal therapy (PTT; Figure 6K). This synergistic effect highlighted a new type of core–shell MOF nanostructure as a multifunctional nanoplatform for cancer targeting.

Porphyrinic MOF-based photodynamic cancer therapy

Although many MOF-based drug delivery systems have been developed, there are challenges associated with traditional chemotherapy like drug resistance and side effects that need to be addressed. Considerable effort has been done to the fabrication of multifunctional therapeutic agents. The emergence of MOF-based functional nanomaterials provided opportunities to mitigate these challenges. In this section, we focus our discussion on porphyrinic MOF-based nanostructures, which have garnered significant attention in nanomedicine.

Porphyrin derivatives are widely used as photosensitizers for photodynamic therapy (PDT); however, the effective delivery of the porphyrinic molecules to tumor sites is complicated by their instability and intrinsic hydrophobic properties. To address these problems, various nanoparticle carriers have been explored for loading different kinds of porphyrinic photosensitizers, including porous MOFs or porous silica [85,97]. However, the loading efficiencies were generally poor. In porous silica, for example, the loading of porphyrinic photosensitizers was only 0.34%, which limits the generation of singlet oxygen and makes it difficult for therapeutic application [98]. Aside from the low loading efficiency, the molecule photosensitizers could also diffuse out of the nanocarriers easily during the delivery process, resulting in lower PDT efficacy.

One way to overcome the low loading efficiency is by incorporating the porphyrinic molecules directly into the MOF structures where the porphyrinic photosensitizers were used as building blocks for the MOF scaffold. The Lin and Zhou groups have leveraged this strategy to produce excellent results [99–103]. These porphyrinic incorporated MOFs solved the poor solubility, self-quenching and aggregation problems associated with photosensitizer molecules. Moreover, they can efficiently produce singlet oxygen for PDT. The first DBP-UiO porphyrinic MOFs used for PDT was reported by Lin and colleagues in 2014 [99]. The DBP-UiO porphyrinic MOFs adopted a UiO-type structure and was constructed by porphyrin derivative, 5,15-di(p-benzoato)porphyrin (H_2DBP) and $HfCl_4$. TEM image showed the DBP-UiO particles had a plate morphology with approximately 100 nm in diameter and approximately 10 nm in thickness (Figure 7A). The DBP-UiO particles still possessed the strong light absorption ability of the H_2DBP ligand and demonstrated high singlet oxygen generation ability upon red light irradiation (Figure 7B). The *in vivo* experiments confirmed that the DBP-UiO MOFs worked as an excellent PDT photosensitizer (Figure 7C). In comparison, no therapeutic effect was observed in the mice that were treated with the ligand H_2DBP. This work demonstrated that the nanoscale porphyrinic MOFs could be used as potential PDT agents for cancer therapy. In this regard, other kinds of porphyrinic MOF nanomaterials have since been reported for PDT due to their structural and chemical tunability [100–106].

Zhou and colleagues showed size-dependent targeted PDT with porphyrinic PCN-224 (Zr-MOFs) nanoparticles (porous coordination network [PCN]) [102]. The PCN-224 MOFs nanoparticles were constructed from tetrakis(4-carboxyphenyl)porphyrin and zirconyl chloride. These particles exhibited good chemical stability and have porous channels that allow diffusion of the molecular oxygen (Figure 7D). By fine-tuning the reaction conditions, the size of the PCN-224 can change from approximately 30 to 190 nm. Notably, the PCN-224 maintained their singlet-

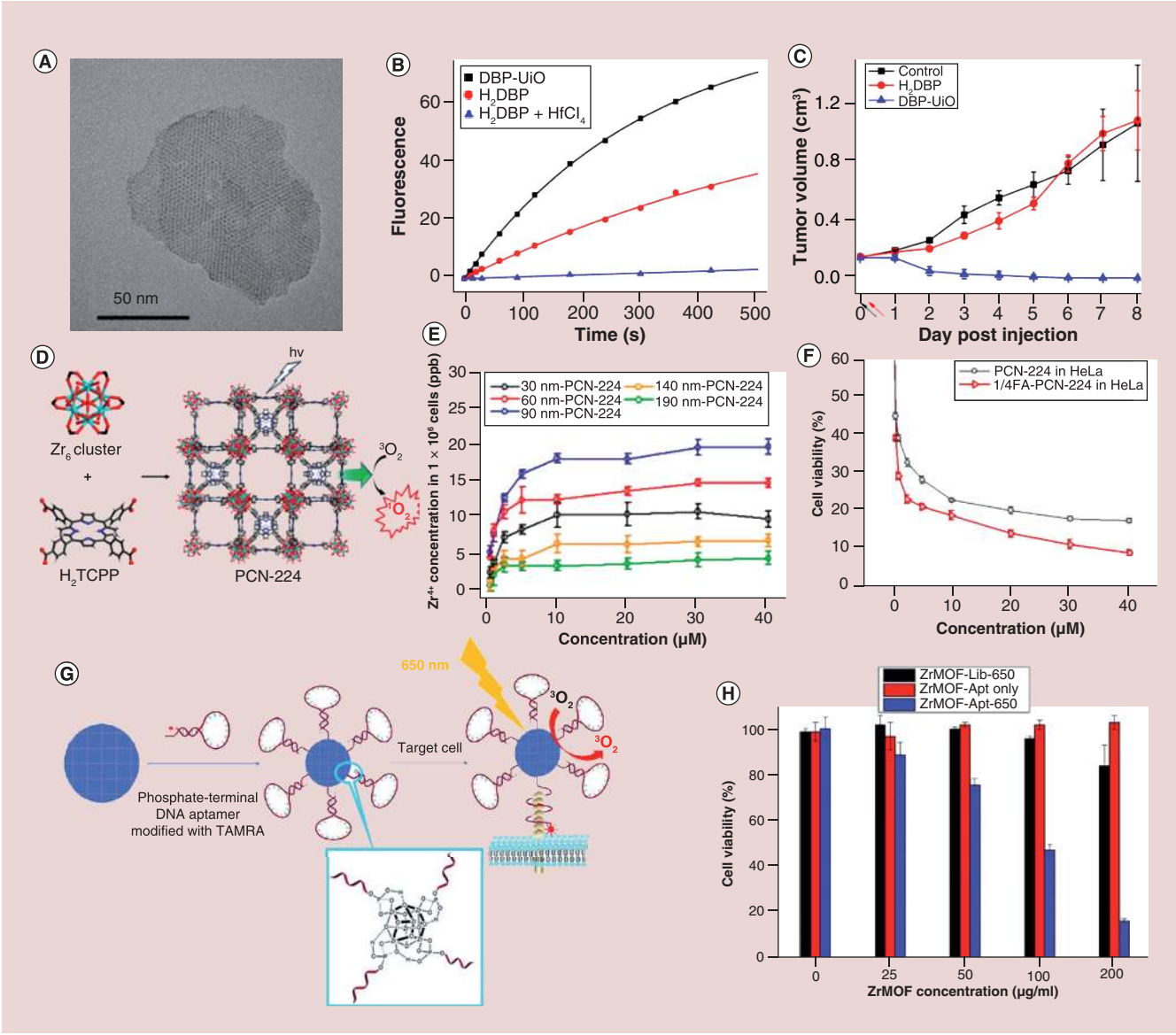

Figure 7. The porphyrinic metal-organic frameworks for photodynamic therapy. (A) Transmission electron microscopy image of DBP-UiO MOFs nanoplate. **(B)** Singlet-oxygen generation from DBP-UiO MOFs, H_2DBP and H_2DBP+$HfCl_4$. **(C)** Tumor growth curve of the photodynamic therapy treatment on SQ20B tumor-bearing mice (black and red arrows refer to the injection and irradiation time points). **(D)** 3D nanoporous structure of the PCN-224 MOFs. **(E)** Cellular uptake of different size PCN-224 MOFs nanoparticles at various concentrations (incubation 24 h). **(F)** *In vitro* PDT efficacy of PCN-224 MOFs nanoparticles (with and without folic acid functionalization) cultured HeLa cells. **(G)** Scheme of phosphate-terminal DNA aptamer conjugated Zr-MOFs nanoparticle quencher. **(H)** Cell viability tests of HeLa cells were cultured with Zr-MOF-library or Zr-MOF-aptamer nanoparticles and irradiated with 650-nm laser light for 5 min (200 mW/cm^2), for Zr-MOF-aptamer only, the HeLa cells were cultured Zr-MOF-aptamer nanoparticles without laser irradiation.
DBP: Di(*p*-benzoato)porphyrin; MOF: Metal-organic framework; PCN: Porous coordination network; UiO: Universitetet i Oslo.

oxygen generation ability regardless of size. The PCN-224 MOFs were functionalized with folic acid to target the folate receptor, which is overexpressed in many cancers. HeLa cells were cultured with PCN-224 nanoparticles ranging from approximately 30 to 190 nm in size. A plateau around 12 h was observed in the cellular uptake studies, and the approximately 90-nm-sized PCN-224 showed the highest uptake in the HeLa cells (Figure 7E). Under 630-nm light irradiation, the approximately 90-nm PCN-224 nanoparticles functionalized with folic acid demonstrated cytotoxicity than the nonfunctionalized derivative (Figure 7F).

For porphyrinic MOF nanoparticles, the intrinsic fluorescence of the nanoparticles can be used for imaging. However, relying on the enhanced permeability and retention effect alone is limited by high background uptake [107]. Molecular-targeted imaging can be used to ameliorate tumor uptake and in turn signal-to-noise ratios. For example, MOF nanoparticles can be conjugated with small molecules, peptides or aptamers to target specific receptors on the cell surface and be taken up by receptor-mediated endocytosis, resulting in enhanced uptake in the tumor sites [102,107,108]. Liu *et al.* developed DNA aptamer-conjugated Zr-MOF (PCN-224) nanoparticles for molecular-targeted imaging and PDT (Figure 7G) [107]. In their design, the TAMRA-modified phosphate-terminal aptamer was conjugated onto the surface of the Zr-MOFs nanoparticles through the unsaturated coordination Zr6 cluster sites. Based on π–π stacking-induced quenching of TAMRA by Zr-MOF nanoparticles, no visible signal can be detected until a binding event took place. Binding with the target led to a conformational change for the aptamer and resulted in the fluorescence recovery of TAMRA. In PDT studies, the aptamer-conjugated Zr-MOF nanoparticles with significantly enhanced cytotoxic effect in HeLa cells compared with PCN-224 particles conjugated with control aptamer sequence (Figure 7H).

The efficacy of the PDT by MOFs is limited by tumor hypoxia [103]. To solve the problem, Lin and colleagues reported a Fe_3O cluster-based porphyrinic MOFs (Fe-TBP), which could decompose the intracellular H_2O_2 to produce O_2 through a Fenton-like reaction. The produced oxygen was further converted to singlet oxygen by the Fe-TBP under red light irradiation (Figure 8A & B) [103]. The authors treated CT26 tumor-bearing mice with Fe-TBP in combination with an α-PD-L1 antibody. This treatment significantly induced the expansion of both $CD4^+$ helper and $CD8^+$ cytotoxic T cells and resulted in the regression of primary and distant tumors (Figure 8C).

The materials with NIR absorption are the good candidates for *in vivo* imaging. NIR light can penetrate biological tissues such as skin and blood more efficiently than visible light. Nanomaterials such as rare-earth doped upconversion nanoparticles (UCNPs) with NIR absorption have received scientific focus [110]. The UCNPs that can absorb long wavelength light and emit short wavelength light, are very promising nanoprobes for imaging owing to their excellent NIR excitable upconversion luminescence properties [85,87,111–114]. Recently, He *et al.* reported a novel core-satellite porphyrinic MOF-UCNP nanoassembly using DNA template for efficient PDT (Figure 8D) [109]. The porphyrinic MOFs, composed from Zr6 cluster and tetratopic linker, possessed a 3D nanoporous framework structure for singlet-oxygen diffusion. UCNPs in the core-satellite not only offered NIR imaging capability but also emitted light to excite porphyrinic MOF to generate singlet oxygen due to the overlap of UV–vis spectra of MOFs and photoluminescence spectra of UCNPs. Compared with the mixture of MOF and UCNP (25.1%), the core-satellite assembly (57.9%) showed much better performance in producing singlet oxygen (Figure 8E). This was due to the improved the energy transfer from the UCNPs to the MOFs for singlet-oxygen production. The *in vitro* studies also confirmed that the core-satellite MOF-UCNP nanoassemblies had the best performance for cancer cell therapy compared with the MOF and UCNP mixture samples. By integrating photothermal conversion materials such as gold nanorods, the porphyrinic MOFs can be used for chemotherapy, PDT and PTT [115].

MOF-based theranostics

Theranostics means the combination of diagnostics and therapeutics. Different from multistep procedures, it aims to eliminate steps and improve treatment efficacy [116–118]. It combines the advantages of improved diagnosis, targeted drug delivery and imaging, reduced side effects, of which the MOF-based theranostics have been well explored recently. Wang *et al.* reported the sandwich-like Fe_3O_4@MIL-100(Fe)-UCNPs ($NaYF_4$:Yb,Tm@$NaGdF_4$:Yb) nanostructures for computed tomography and upconversion luminescence imaging-guided cancer therapy [119]. In their work, they used a layer-by-layer strategy to synthesize the Fe_3O_4@MIL-100(Fe) nanoparticles as the photosensitizer. Then, the amine-modified UCNPs were conjugated onto the Fe_3O_4@MIL-100(Fe) nanoparticles through the carboxyl groups on the MIL-100(Fe) surface. Under 980-nm laser irradiation, the UCNPs transferred the emitted visible/UV light to the nanoparticles photosensitizer to produce cytotoxic hydroxyl radicals for tumor therapy. The *in vivo* studies showed that therapeutic treatment could be guided by the computed tomography and upconversion luminescence imaging. Chen *et al.* reported intrinsically radioactive UiO-66 nanoparticles for

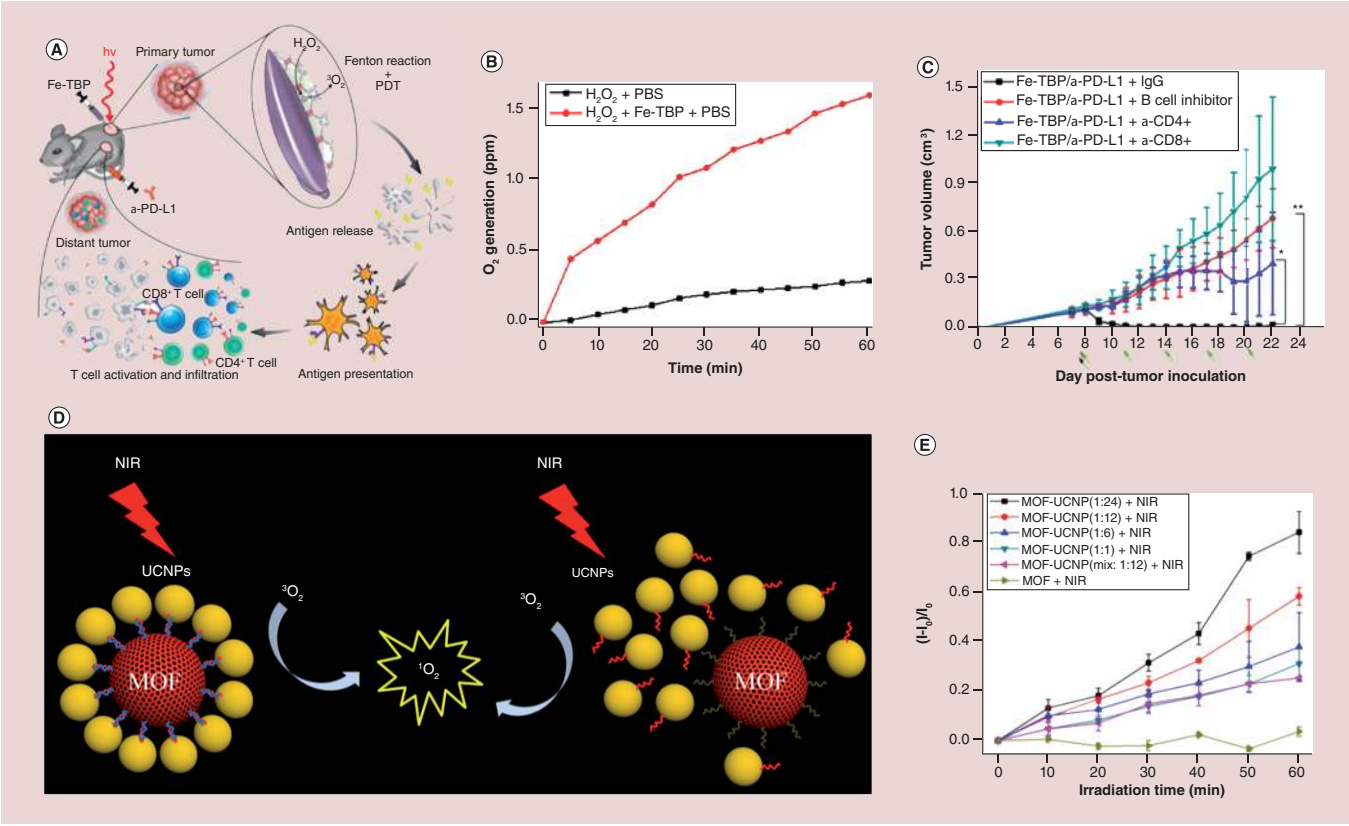

Figure 8. The porphyrinic metal-organic frameworks and metal-organic framework-based nanomaterials for photodynamic therapy.
(A) Scheme of using Fe-TBP MOFs to overcome hypoxia for PDT-primed cancer immunotherapy. **(B)** Time-dependent oxygen generation. **(C)** Tumor growth curves of CT26 tumor-bearing mice with T-cell or B-cell depletion. **(D)** Scheme of the core-satellite MOF-UCNPs assemblies and the mixture of the MOF-UCNPs. **(E)** Singlet-oxygen production from the MOF-UCNPs with different ratios.
MOF: Metal-organic framework; NIR: Near infrared; PDT: Photodynamic therapy; TBP: 5,10,15,20-tetra(p-benzoato)porphyrin; UCNP: Upconversion nanoparticle.
(A) Reproduced with permission from [103] © American Chemical Society (2018).
(B) Reproduced with permission from [103] © American Chemical Society (2018).
(C) Reproduced with permission from [103] © American Chemical Society (2018).
(D) Reproduced with permission from [109] © WILEY-VCH Verlag GmbH & Co. KGaA, Weinheim (2017).
(E) Reproduced with permission from [109] © WILEY-VCH Verlag GmbH & Co. KGaA, Weinheim (2017).

in vivo positron emission tomography imaging [120]. In this work, the radioactive Zirconium chloride (UiO-66 precursor) was used to construct the UiO-66 nanoparticles. DOX was then loaded onto the UiO-66 with a high loading efficiency of 50%. The toxicity evaluation showed that the PEGylated UiO-66 had no acute or chronic toxicity. The intrinsically properties and easy functionalities of the MOFs make them very promising for field of theranostics nanomedicine.

Conclusion

In summary, we reviewed recent advances in MOFs for drug delivery and cancer therapy, from individual MOF to multifunctionalized MOF hybrids. MOF-based nanomaterials are attractive platforms due to their high surface area, tunable pore size and structure, and versatile functionality. MOFs can be used to delivery cytotoxic payloads, or to mediate PDT or PTT. At the same time, the composition of MOFs can be customized for imaging applications (e.g., metals for MRI or porphyrin for fluorescence imaging) as well. Although MOFs hold promise for biomedical applications, researchers should be cognizant of barriers that may undermine their translatability. First, many MOF materials are not very stable at low pH due to the weak coordination interactions within the constructed structure. While this feature can be desirable for pH-responsive systems, it can lead to premature drug release and undesired toxicity in other cases. Investigations of the degradation mechanisms of different classes of MOF will greatly benefit the design and synthesis of new MOF carriers. Second, more vigilant research is required to better understand the

systemic toxicity associated with MOFs. These studies are crucial for determining therapeutic indices, especially if MOFs are to be implemented in the clinic. We expect that those challenges will stimulate the nanomedicine community to innovate multifunctional MOFs that are safe and effective.

Future perspective

Considering the rapid increasing demands of nanoscale MOFs for nanomedicine, intrinsic properties, such as the stability, toxicity, and biocompatibility of MOFs and external properties from guests, need to be paid more attentions when extending the functions of MOFs. The stability determines the biomedical applications. Poor stability in physiological conditions typically causes lots of issues, such as decomposition of MOF carriers, premature drug release, short circulation time and serious side effects. Thus, stable MOFs can offer robust and efficient drug carriers. Efforts have been done in order to improve the stability and biocompatibility of MOF materials [121,122].

On the other hand, nontoxic or less toxic MOFs with good biocompatibility can significantly facilitate their biomedical applications. Ligands and metal ions with minimum toxicity are more favored when constructing MOFs. Surface coating with silica, PEG and DNA not only improves the stability of MOFs but also helps achieve a targeted delivery to improve the therapy efficiency and decrease the side effects. To data, there have been only few reports about the safety of MOFs, and more efforts are needed to evaluate the acute and chronic toxicities of MOFs [123–125]. Furthermore, MOF-based bioimaging and theranostic applications are far from the clinical requirements in its current status due to the lack of deep understanding in metabolism and excretion for the MOF materials [107]. We envision that these challenges will motivate us to create more innovative multifunctional MOF-based nanomedicines.

Executive summary

Individual nanoscale metal-organic framework for drug delivery

- High surface area of metal-organic framework (MOF) nanomaterials can be taken advantage of to maximize the drug-loading efficiencies.
- Postencapsulation method can be used for loading drugs with dimensions smaller than the sizes of MOF channels and pores.
- The *in situ* drug encapsulation method prevents the leakage of loaded drug/cargo and also expands the selection of MOFs for various sized drug molecules.

Functional MOF nanocompositions for drug delivery

- The acid unstable MOF feature can be used for pH-responsive drug release.
- Surface modification is a good option to achieve additional functionalities for stimuli-responsive drug release for MOF materials.
- The integration of plasmonic noble metal/magnetic nanoparticles endows the MOF nanomaterials as photothermal/MRI agents.

Porphyrinic MOF-based photodynamic cancer therapy

- Porphyrinic MOFs show better photodynamic therapy efficacy than porphyrin-derived molecules.
- Porphyrinic MOF-based functional nanomaterials provide opportunities as theranostics.

Financial & competing interests disclosure

This work was supported by the Intramural Research Program, National Institute of Biomedical Imaging and Bioengineering, the National Natural and Science Foundation of China (Nos. 81527803, 81420108018), the Ministry of Science and Technology Key Research and Development Plan in 13th Five-year of China (SQ2018YFC010090) and Zhejiang Science and Technology Project (No. 2019C03077). The authors have no relevant affiliations or financial involvement with any organization or entity with a financial interest in or financial conflict with the subject matter or materials discussed in the manuscript. This includes employment, consultancies, honoraria, stock ownership or options, expert testimony, grants or patents received or pending, or royalties.

No writing assistance was utilized in the production of this manuscript.

References

Papers of special note have been highlighted as: • of interest; •• of considerable interest

1. Wu M-X, Yang Y-W. Metal-organic framework (MOF)-based drug/cargo delivery and cancer therapy. *Adv. Mater.* 29(23), 1606134 (2017).

• **A review paper also introduced recent progress of metal-organic framework (MOF) materials in drug delivery.**

2. Wang Y, Zhao Q, Han N *et al.* Mesoporous silica nanoparticles in drug delivery and biomedical applications. *Nanomed. Nanotechnol.* 11(2), 313–327 (2015).
3. Liu H, Chen D, Li L *et al.* Multifunctional gold nanoshells on silica nanorattles: a platform for the combination of photothermal therapy and chemotherapy with low systemic toxicity. *Angew. Chem. Int. Ed.* 50(4), 891–895 (2011).
4. Liu H, Liu T, Wu X *et al.* Targeting gold nanoshells on silica nanorattles: a drug cocktail to fight breast tumors via a single irradiation with near-infrared laser light. *Adv. Mater.* 24(6), 755–761 (2012).
5. Zebibula A, Alifu N, Xia L *et al.* Ultrastable and biocompatible NIR-II quantum dots for functional bioimaging. *Adv. Funct. Mater.* 28(9), 1703451 (2018).
6. Guo T, Wu Y, Lin Y *et al.* Black phosphorus quantum dots with renal clearance property for efficient photodynamic therapy. *Small* 14(4), 1702815 (2018).
7. Wang W, Cheng D, Gong F, Miao X, Shuai X. Design of multifunctional micelle for tumor-targeted intracellular drug release and fluorescent imaging. *Adv. Mater.* 24, 115–120 (2012).
8. Wang HJ, Shrestha R, Zhang Y. Encapsulation of photosensitizers and upconversion nanocrystals in lipid micelles for photodynamic therapy. *Part. Part. Syst. Char.* 31(2), 228–235 (2014).
9. Rodríguez-Pulido A, Kondrachuk AI, Prusty DK *et al.* Light-triggered sequence-specific cargo release from DNA block copolymer-lipid vesicles. *Angew. Chem. Int. Ed.* 52(3), 1008–1012 (2013).
10. Wang H, Zhao P, Su W *et al.* PLGA/polymeric liposome for targeted drug and gene co-delivery. *Biomaterials* 31(33), 8741–8748 (2010).
11. Wang H, Zhao P, Liang X *et al.* Folate-PEG coated cationic modified chitosan – cholesterol liposomes for tumor-targeted drug delivery. *Biomaterials* 31(14), 4129–4138 (2010).
12. Wang H, Zhang S, Liao Z *et al.* PEGlated magnetic polymeric liposome anchored with TAT for delivery of drugs across the blood-spinal cord barrier. *Biomaterials* 31(25), 6589–6596 (2010).
13. Wang X, Cai X, Hu J *et al.* Glutathione-triggered "Off-On" release of anticancer drugs from dendrimer-encapsulated gold nanoparticles. *J. Am. Chem. Soc.* 135(26), 9805–9810 (2013).
14. Wuttke S, Lismont M, Escudero A, Rungtaweevoranit B, Parak WJ. Positioning metal-organic framework nanoparticles within the context of drug delivery – a comparison with mesoporous silica nanoparticles and dendrimers. *Biomaterials* 123, 172–183 (2017).
15. Raeesi V, Chou LYT, Chan WCW. Tuning the drug loading and release of DNA-assembled gold-nanorod superstructures. *Adv. Mater.* 28(38), 8511–8518 (2016).
16. Diercks CS, Yaghi OM. The atom, the molecule, and the covalent organic framework. *Science* 355(6328), pii: eaal1585 (2017).
17. Li H, Eddaoudi M, O'keeffe M, Yaghi OM. Design and synthesis of an exceptionally stable and highly porous metal-organic framework. *Nature* 402(6759), 276–279 (1999).
18. Kong X, Deng H, Yan F *et al.* Mapping of functional groups in metal-organic frameworks. *Science* 341(6148), 882–885 (2013).
19. Horcajada P, Chalati T, Serre C *et al.* Porous metal-organic-framework nanoscale carriers as a potential platform for drug delivery and imaging. *Nat. Mater.* 9(2), 172–178 (2010).
20. Baati T, Njim L, Neffati F *et al.* In depth analysis of the *in vivo* toxicity of nanoparticles of porous iron(iii) metal-organic frameworks. *Chem. Sci.* 4(4), 1597–1607 (2013).
21. Wuttke S, Zimpel A, Bein T *et al.* Validating metal-organic framework nanoparticles for their nanosafety in diverse biomedical applications. *Adv. Healthcare Mater.* 6(2), 1600818 (2016).
22. Freund R, Lächelt U, Gruber T, Rühle B, Wuttke S. Multifunctional efficiency: extending the concept of atom economy to functional nanomaterials. *ACS Nano* 12(3), 2094–2105 (2018).
23. Furukawa H, Cordova KE, O'keeffe M, Yaghi OM. The chemistry and applications of metal-organic frameworks. *Science* 341(6149), 1230444 (2013).
24. Lismont M, Dreesen L, Wuttke S. Metal-organic framework nanoparticles in photodynamic therapy: current status and perspectives. *Adv. Funct. Mater.* 27(14), 1606314 (2017).
25. Dong Z, Sun Y, Chu J, Zhang X, Deng H. Multivariate metal-organic frameworks for dialing-in the binding and programming the release of drug molecules. *J. Am. Chem. Soc.* 139(40), 14209–14216 (2017).
26. Preiß T, Zimpel A, Wuttke S, Rädler OJ. Kinetic analysis of the uptake and release of fluorescein by metal-organic framework nanoparticles. *Materials* 10(2), 216 (2017).
27. Horcajada P, Serre C, Vallet-Regí M *et al.* Metal-organic frameworks as efficient materials for drug delivery. *Angew. Chem. Int. Ed.* 45(36), 5974–5978 (2006).

• **The first exploratory report used MOF as a drug carrier.**

28. Muñoz B, Rámila A, Pérez-Pariente J, Díaz I, Vallet-Regí M. MCM-41 organic modification as drug delivery rate regulator. *Chem. Mater.* 15(2), 500–503 (2003)

29. Horcajada P, Serre C, Maurin G *et al.* Flexible porous metal-organic frameworks for a controlled drug delivery. *J. Am. Chem. Soc.* 130(21), 6774–6780 (2008).
30. An J, Geib SJ, Rosi NL. Cation-triggered drug release from a porous zinc-adeninate metal-organic framework. *J. Am. Chem. Soc.* 131(24), 8376–8377 (2009).
31. Sun C-Y, Qin C, Wang C-G *et al.* Chiral nanoporous metal-organic frameworks with high porosity as materials for drug delivery. *Adv. Mater.* 23(47), 5629–5632 (2011).
32. Sun C-Y, Qin C, Wang X-L *et al.* Zeolitic imidazolate framework-8 as efficient pH-sensitive drug delivery vehicle. *Dalton Trans.* 41(23), 6906–6909 (2012).
33. Cunha D, Ben Yahia M, Hall S *et al.* Rationale of drug encapsulation and release from biocompatible porous metal-organic frameworks. *Chem. Mater.* 25(14), 2767–2776 (2013).
34. He C, Lu K, Liu D, Lin W. Nanoscale metal-organic frameworks for the co-delivery of cisplatin and pooled siRNAs to enhance therapeutic efficacy in drug-resistant ovarian cancer cells. *J. Am. Chem. Soc.* 136(14), 5181–5184 (2014).
35. Illes B, Wuttke S, Engelke H. Liposome-coated iron fumarate metal-organic framework nanoparticles for combination therapy. *Nanomaterials* 7(11), pii: E351 (2017).
36. Duan Y, Ye F, Huang Y *et al.* One-pot synthesis of a metal-organic framework-based drug carrier for intelligent glucose-responsive insulin delivery. *Chem. Commun.* 54(42), 5377–5380 (2018).
37. Chen Y, Li P, Modica JA, Drout RJ, Farha OK. Acid-resistant mesoporous metal-organic framework toward oral insulin delivery: protein encapsulation, protection, and release. *J. Am. Chem. Soc.* 140(17), 5678–5681 (2018).
38. Liu W-G, Truhlar DG. Computational linker design for highly crystalline metal-organic framework NU-1000. *Chem. Mater.* 29(19), 8073–8081 (2017).
39. Chen W-H, Luo G-F, Vázquez-González M *et al.* Glucose-responsive metal-organic-framework nanoparticles act as "Smart" sense-and-treat carriers. *ACS Nano* 12(8), 7538–7545 (2018).
40. Teplensky MH, Fantham M, Li P *et al.* Temperature treatment of highly porous Zirconium-containing metal-organic frameworks extends drug delivery release. *J. Am. Chem. Soc.* 139(22), 7522–7532 (2017).
41. Motakef-Kazemi N, Shojaosadati SA, Morsali A. *In situ* synthesis of a drug-loaded MOF at room temperature. *Micropor. Mesopor. Mater.* 186, 73–79 (2014).
42. Zhuang J, Kuo C-H, Chou L-Y *et al.* Optimized metal-organic-framework nanospheres for drug delivery: evaluation of small-molecule encapsulation. *ACS Nano* 8(3), 2812–2819 (2014).
43. Park KS, Ni Z, Cote AP *et al.* Exceptional chemical and thermal stability of zeolitic imidazolate frameworks. *Proc. Natl Acad. Sci. USA* 103(27), 10186–10191 (2006).
44. Shieh F-K, Wang S-C, Yen C-I *et al.* Imparting functionality to biocatalysts via embedding enzymes into nanoporous materials by a de Novo approach: size-selective sheltering of catalase in metal-organic framework microcrystals. *J. Am. Chem. Soc.* 137(13), 4276–4279 (2015).
45. Morris W, Doonan CJ, Furukawa H, Banerjee R, Yaghi OM. Crystals as molecules: postsynthesis covalent functionalization of zeolitic imidazolate frameworks. *J. Am. Chem. Soc.* 130(38), 12626–12627 (2008).
46. Alsaiari SK, Patil S, Alyami M *et al.* Endosomal escape and delivery of CRISPR/Cas9 genome editing machinery enabled by nanoscale zeolitic imidazolate framework. *J. Am. Chem. Soc.* 140(1), 143–146 (2018).
47. Zheng H, Zhang Y, Liu L *et al.* One-pot synthesis of metal-organic frameworks with encapsulated target molecules and their applications for controlled drug delivery. *J. Am. Chem. Soc.* 138(3), 962–968 (2016).

•• ***In situ* encapsulation of drug molecules into MOF matrix for controlled drug release.**

48. Horcajada P, Chalati T, Serre C *et al.* Porous metal-organic-framework nanoscale carriers as a potential platform for drug delivery and imaging. *Nat. Mater.* 9(2), 172–178 (2010).
49. Chulkaivalsucharit P, Wu X, Ge J. Synthesis of enzyme-embedded metal-organic framework nanocrystals in reverse micelles. *RSC Adv.* 5(123), 101293–101296 (2015).
50. Liang K, Ricco R, Doherty CM *et al.* Biomimetic mineralization of metal-organic frameworks as protective coatings for biomacromolecules. *Nat. Commun.* 6, Article no. 7240 (2015).
51. Wu X, Ge J, Yang C, Hou M, Liu Z. Facile synthesis of multiple enzyme-containing metal-organic frameworks in a biomolecule-friendly environment. *Chem. Commun.* 51(69), 13408–13411 (2015).
52. Zhang Y, Wang F, Ju E *et al.* Metal-organic-framework-based vaccine platforms for enhanced systemic immune and memory response. *Adv. Funct. Mater.* 26(35), 6454–6461 (2016).
53. Lyu F, Zhang Y, Zare RN, Ge J, Liu Z. One-pot synthesis of protein-embedded metal-organic frameworks with enhanced biological activities. *Nano Lett.* 14(10), 5761–5765 (2014).
54. He L, Liu Y, Liu J *et al.* Core-shell noble-metal@metal-organic-framework nanoparticles with highly selective sensing property. *Angew. Chem. Int. Ed.* 52(13), 3741–3745 (2013).

55. Lu G, Li S, Guo Z *et al.* Imparting functionality to a metal-organic framework material by controlled nanoparticle encapsulation. *Nat. Chem.* 4(4), 310–316 (2012).
56. Yang Q, Xu Q, Yu S-H, Jiang H-L. Pd Nanocubes@ZIF-8: integration of plasmon-driven photothermal conversion with a metal-organic framework for efficient and selective catalysis. *Angew. Chem. Int. Ed.* 55(11), 3685–3689 (2016).
57. Buso D, Jasieniak J, Lay MDH *et al.* Highly luminescent metal-organic frameworks through quantum dot doping. *Small* 8(1), 80–88 (2012).
58. Liu Q, Jin L-N, Sun W-Y. Facile fabrication and adsorption property of a nano/microporous coordination polymer with controllable size and morphology. *Chem. Commun.* 48(70), 8814–8816 (2012).
59. Pan Y, Heryadi D, Zhou F *et al.* Tuning the crystal morphology and size of zeolitic imidazolate framework-8 in aqueous solution by surfactants. *CrystEngComm* 13(23), 6937–6940 (2011).
60. Lu G, Cui C, Zhang W, Liu Y, Huo F. Synthesis and self-assembly of monodispersed metal-organic framework microcrystals. *Chem. Asian. J.* 8(1), 69–72 (2013).
61. Rieter WJ, Taylor KML, Lin W. Surface modification and functionalization of nanoscale metal-organic frameworks for controlled release and luminescence sensing. *J. Am. Chem. Soc.* 129(32), 9852–9853 (2007).
62. Röder R, Preiß T, Hirschle P *et al.* Multifunctional nanoparticles by coordinative self-assembly of His-tagged units with metal-organic frameworks. *J. Am. Chem. Soc.* 139(6), 2359–2368 (2017).
63. Liu B, Ma M, Zacher D *et al.* Chemistry of SURMOFs: layer-selective installation of functional groups and post-synthetic covalent modification probed by fluorescence microscopy. *J. Am. Chem. Soc.* 133(6), 1734–1737 (2011).
64. Zimpel A, Preiß T, Röder R *et al.* Imparting functionality to MOF nanoparticles by external surface selective covalent attachment of polymers. *Chem. Mater.* 28(10), 3318–3326 (2016).
65. Kondo M, Furukawa S, Hirai K, Kitagawa S. Coordinatively immobilized monolayers on porous coordination polymer crystals. *Angew. Chem. Int. Ed.* 49(31), 5327–5330 (2010).
66. Wang X-G, Dong Z-Y, Cheng H *et al.* A multifunctional metal-organic framework based tumor targeting drug delivery system for cancer therapy. *Nanoscale* 7(38), 16061–16070 (2015).
67. Tan L-L, Li H, Qiu Y-C *et al.* Stimuli-responsive metal-organic frameworks gated by pillar [5]arene supramolecular switches. *Chem. Sci.* 6(3), 1640–1644 (2015).
68. Illes B, Hirschle P, Barnert S *et al.* Exosome-coated metal-organic framework nanoparticles: an efficient drug delivery platform. *Chem. Mater.* 29(19), 8042–8046 (2017).
69. Wuttke S, Braig S, Preiß T *et al.* MOF nanoparticles coated by lipid bilayers and their uptake by cancer cells. *Chem. Commun.* 51(87), 15752–15755 (2015).
70. Taylor-Pashow KML, Rocca JD, Xie Z, Tran S, Lin W. Postsynthetic modifications of iron-carboxylate nanoscale metal-organic frameworks for imaging and drug delivery. *J. Am. Chem. Soc.* 131(40), 14261–14263 (2009).
71. Xing L, Cao Y, Che S. Synthesis of core-shell coordination polymer nanoparticles (CPNs) for pH-responsive controlled drug release. *Chem. Commun.* 48(48), 5995–5997 (2012).
72. Abánades Lázaro I, Haddad S, Sacca S *et al.* Selective surface PEGylation of UiO-66 nanoparticles for enhanced stability, cell uptake, and pH-Responsive drug delivery. *Chem* 2(4), 561–578 (2017).
73. Morris W, Briley WE, Auyeung E, Cabezas MD, Mirkin CA. Nucleic acid-metal organic framework (MOF) nanoparticle conjugates. *J. Am. Chem. Soc.* 136(20), 7261–7264 (2014).
74. Chen W-H, Yu X, Cecconello A *et al.* Stimuli-responsive nucleic acid-functionalized metal-organic framework nanoparticles using pH- and metal-ion-dependent DNAzymes as locks. *Chem. Sci.* 8(8), 5769–5780 (2017).
75. Chen WH, Liao WC, Sohn Yang S *et al.* Stimuli-responsive nucleic acid-based polyacrylamide hydrogel-coated metal-organic framework nanoparticles for controlled drug release. *Adv. Funct. Mater.* 28(8), 1705137 (2018).
76. Lei B, Wang M, Jiang Z *et al.* Constructing redox-responsive metal-organic framework nanocarriers for anticancer drug delivery. *ACS Appl. Mater. Inter.* 10(19), 16698–16706 (2018).
77. Meng X, Gui B, Yuan D, Zeller M, Wang C. Mechanized azobenzene-functionalized zirconium metal-organic framework for on-command cargo release. *Sci. Adv.* 2(8), e1600480 (2016).
78. Tan L-L, Li H, Zhou Y *et al.* Zn^{2+}-triggered drug release from biocompatible Zirconium MOFs equipped with supramolecular gates. *Small* 11(31), 3807–3813 (2015).
79. Tan L-L, Song N, Zhang SX-A *et al.* Ca^{2+}, pH and thermo triple-responsive mechanized Zr-based MOFs for on-command drug release in bone diseases. *J. Mater. Chem. B.* 4(1), 135–140 (2016).
80. Shen Z, Song J, Zhou Z *et al.* Dotted core-shell nanoparticles for T1-eeighted MRI of tumors. *Adv. Mater.* 30(33), 1803163 (2018).
81. Xing R, Bhirde A, Wang S *et al.* Hollow iron oxide nanoparticles as multidrug resistant drug delivery and imaging vehicles. *Nano Res.* 6(1), 1–9 (2013).

82. Lin L-S, Song J, Yang H-H, Chen X. Yolk-shell nanostructures: design, synthesis, and biomedical applications. *Adv. Mater.* 30(6), 1704639 (2018).

83. Li Y, Tang J, He L *et al.* Core-shell upconversion nanoparticle@metal-organic framework nanoprobes for luminescent/magnetic dual-mode targeted imaging. *Adv. Mater.* 27(27), 4075–4080 (2015).

84. He L, Mao C, Brasino M *et al.* TiO_2-capped gold nanorods for plasmon-enhanced production of reactive oxygen species and photothermal delivery of chemotherapeutic agents. *ACS Appl. Mater. Inter.* 10(33), 27965–27971 (2018).

85. He L, Dragavon J, Cho S *et al.* Self-assembled gold nanostar-$NaYF_4$:Yb/Er clusters for multimodal imaging, photothermal and photodynamic therapy. *J. Mater. Chem. B* 4(25), 4455–4461 (2016).

86. Wang S, Huang P, Nie L *et al.* Single continuous wave laser induced photodynamic/plasmonic photothermal therapy using photosensitizer-functionalized gold nanostars. *Adv. Mater.* 25(22), 3055–3061 (2013).

87. Chen G, Qiu H, Prasad PN, Chen X. Upconversion nanoparticles: design, nanochemistry, and applications in theranostics. *Chem. Rev.* 114(10), 5161–5214 (2014).

88. Yang Z, Tian R, Wu J *et al.* Impact of semiconducting perylene diimide nanoparticle size on lymph node mapping and cancer imaging. *ACS Nano* 11(4), 4247–4255 (2017).

89. Yang Z, Dai Y, Yin C *et al.* Activatable semiconducting theranostics: simultaneous generation and ratiometric photoacoustic imaging of reactive oxygen species *in vivo*. *Adv. Mater.* 30(23), 1707509 (2018).

90. Ke F, Yuan Y-P, Qiu L-G *et al.* Facile fabrication of magnetic metal-organic framework nanocomposites for potential targeted drug delivery. *J. Mater. Chem.* 21(11), 3843–3848 (2011).

91. Wu Y-N, Zhou M, Li S *et al.* Magnetic metal-organic frameworks: γ-Fe_2O_3@MOFs via confined *in situ* pyrolysis method for drug delivery. *Small* 10(14), 2927–2936 (2014).

92. He M, Zhou J, Chen J *et al.* Fe_3O_4@carbon@zeolitic imidazolate framework-8 nanoparticles as multifunctional pH-responsive drug delivery vehicles for tumor therapy *in vivo*. *J. Mater. Chem. B* 3(46), 9033–9042 (2015).

93. Zhao H-X, Zou Q, Sun S-K *et al.* Theranostic metal-organic framework core-shell composites for magnetic resonance imaging and drug delivery. *Chem. Sci.* 7(8), 5294–5301 (2016).

94. Li Y, Jin J, Wang D *et al.* Coordination-responsive drug release inside gold nanorod@metal-organic framework core-shell nanostructures for near-infrared-induced synergistic chemo-photothermal therapy. *Nano Research* 11(6), 3294–3305 (2018).

95. Deng K, Hou Z, Li X *et al.* Aptamer-mediated up-conversion core/MOF shell nanocomposites for targeted drug delivery and cell imaging. *Sci. Rep.* 5, 7851 (2015).

96. Yang D, Xu J, Yang G *et al.* Metal-organic frameworks join hands to create an anti-cancer nanoplatform based on 808 nm light driving up-conversion nanoparticles. *Chem. Eng. J.* 344, 363–374 (2018).

97. Zhang L, Lei J, Ma F *et al.* A porphyrin photosensitized metal-organic framework for cancer cell apoptosis and caspase responsive theranostics. *Chem. Commun.* 51(54), 10831–10834 (2015).

98. Idris NM, Gnanasammandhan MK, Zhang J *et al. In vivo* photodynamic therapy using upconversion nanoparticles as remote-controlled nanotransducers. *Nat. Med.* 18(10), 1580–1585 (2012).

99. Lu K, He C, Lin W. Nanoscale metal-organic framework for highly effective photodynamic therapy of resistant head and neck cancer. *J. Am. Chem. Soc.* 136(48), 16712–16715 (2014).

•• **The first report using nanoscale porphyrinic MOFs for photodynamic therapy (PDT).**

100. Lu K, He C, Lin W. A chlorin-based nanoscale metal-organic framework for photodynamic therapy of colon cancers. *J. Am. Chem. Soc.* 137(24), 7600–7603 (2015).

101. Lu K, He C, Guo N *et al.* Chlorin-based nanoscale metal-organic framework systemically rejects colorectal cancers via synergistic photodynamic therapy and checkpoint blockade immunotherapy. *J. Am. Chem. Soc.* 138(38), 12502–12510 (2016).

102. Park J, Jiang Q, Feng D, Mao L, Zhou H-C. Size-controlled synthesis of porphyrinic metal-organic framework and functionalization for targeted photodynamic therapy. *J. Am. Chem. Soc.* 138(10), 3518–3525 (2016).

•• **Reported the facile synthesis and functionalization of PCN-224 porphyrinic MOFs for targeted PDT.**

103. Lan G, Ni K, Xu Z *et al.* Nanoscale metal-organic framework overcomes hypoxia for photodynamic therapy primed cancer immunotherapy. *J. Am. Chem. Soc.* 140(17), 5670–5673 (2018).

104. Zeng J-Y, Zou M-Z, Zhang M *et al.* π-Extended benzoporphyrin-based metal-organic framework for inhibition of tumor metastasis. *ACS Nano* 12(5), 4630–4640 (2018).

105. Zhang H, Tian X-T, Shang Y, Li Y-H, Yin X-B. Theranostic Mn-porphyrin metal-organic frameworks for magnetic resonance imaging-guided nitric oxide and photothermal synergistic therapy. *ACS Appl. Mater. Inter.* 10(34), 28390–28398 (2018).

106. Liu J, Yang Y, Zhu W *et al.* Nanoscale metal-organic frameworks for combined photodynamic & radiation therapy in cancer treatment. *Biomaterials* 97, 1–9 (2016).

107. Liu Y, Hou W, Xia L *et al.* ZrMOF nanoparticles as quenchers to conjugate DNA aptamers for target-induced bioimaging and photodynamic therapy. *Chem. Sci.* 9, 7505–7509 (2018)

108. Ning W, Di Z, Yu Y *et al.* Imparting designer biorecognition functionality to metal-organic frameworks by a DNA-mediated surface engineering strategy. *Small* 14(11), 1703812 (2018).

109. He L, Brasino M, Mao C *et al.* DNA-assembled core-satellite upconverting-metal-organic framework nanoparticle superstructures for efficient photodynamic therapy. *Small* 13(24), 1700504 (2017).

•• **The first research article to integrate upconversion nanoparticles with porphyrinic MOFs for near-infrared light-induced PDT.**

110. Dong H, Du S-R, Zheng X-Y *et al.* Lanthanide nanoparticles: from design toward bioimaging and therapy. *Chem. Rev.* 115(19), 10725–10815 (2015).

111. Park YI, Lee KT, Suh YD, Hyeon T. Upconverting nanoparticles: a versatile platform for wide-field two-photon microscopy and multi-modal *in vivo* imaging. *Chem. Soc. Rev.* 44(6), 1302–1317 (2015).

112. Zhou J, Liu Q, Feng W, Sun Y, Li F. Upconversion luminescent materials: advances and applications. *Chem. Rev.* 115(1), 395–465 (2015).

113. He L, Mao C, Cho S *et al.* Experimental and theoretical photoluminescence studies in nucleic acid assembled gold-upconverting nanoparticle clusters. *Nanoscale* 7(41), 17254–17260 (2015).

114. Li Y, Di Z, Gao J *et al.* Heterodimers made of upconversion nanoparticles and metal-organic frameworks. *J. Am. Chem. Soc.* 139(39), 13804–13810 (2017).

115. Zeng J-Y, Zhang M-K, Peng M-Y, Gong D, Zhang X-Z. Porphyrinic metal-organic frameworks coated gold nanorods as a versatile nanoplatform for combined photodynamic/photothermal/chemotherapy of tumor. *Adv. Funct. Mater.* 28(8), 1705451 (2018).

116. Pradnya Palekar S, Sneha VJ, Manasi MC, Sujata SG. Theranostics for cancer therapy. *Curr. Drug Deliv.* 10(3), 357–362 (2013).

117. Xie J, Lee S, Chen X. Nanoparticle-based theranostic agents. *Adv. Drug Deliv. Rev.* 62(11), 1064–1079 (2010).

118. Peller M, Böll K, Zimpel A, Wuttke S. Metal-organic framework nanoparticles for magnetic resonance imaging. *Inorg. Chem. Front.* 5(8), 1760–1779 (2018).

119. Wang X, Xu J, Yang D *et al.* Fe_3O_4@MIL-100(Fe)-UCNPs heterojunction photosensitizer: rational design and application in near infrared light mediated hypoxic tumor therapy. *Chem. Eng. J.* 354, 1141–1152 (2018).

120. Chen D, Yang D, Dougherty CA *et al. In vivo* targeting and positron emission tomography imaging of tumor with intrinsically radioactive metal-organic frameworks nanomaterials. *ACS Nano* 11(4), 4315–4327 (2017).

121. Li X, Lachmanski L, Safi S *et al.* New insights into the degradation mechanism of metal-organic frameworks drug carriers. *Sci. Rep.* 7(1), 13142 (2017).

122. Gao X, Cui R, Ji G, Liu Z. Size and surface controllable metal-organic frameworks (MOFs) for fluorescence imaging and cancer therapy. *Nanoscale* 10(13), 6205–6211 (2018).

123. Tamames-Tabar C, Cunha D, Imbuluzqueta E *et al.* Cytotoxicity of nanoscaled metal-organic frameworks. *J. Mater. Chem. B* 2(3), 262–271 (2014).

124. Ruyra À, Yazdi A, Espín J *et al.* Synthesis, culture medium stability, and *in vitro* and *in vivo* Zebrafish embryo toxicity of metal-organic framework nanoparticles. *Chem. Eur. J.* 21(6), 2508–2518 (2014).

125. Huxford RC, Dekrafft KE, Boyle WS, Liu D, Lin W. Lipid-coated nanoscale coordination polymers for targeted delivery of antifolates to cancer cells. *Chem. Sci.* 3(1), 198–204 (2012).